1-1-2019

Recent Advances in 3D Graphene Architectures and Their Composites for Energy Storage Applications

Zhijie Wang
University of Wollongong, zw110@uowmail.edu.au

Hong Gao
University of Wollongong, hg173@uowmail.edu.au

Qing Zhang
University of Wollongong, qz964@uowmail.edu.au

Yuqing Liu
University of Wollongong, yuqing@uow.edu.au

Jun Chen
University of Wollongong, junc@uow.edu.au

See next page for additional authors

Recent Advances in 3D Graphene Architectures and Their Composites for Energy Storage Applications

Abstract

Graphene is widely applied as an electrode material in energy storage fields. However, the strong π-π interaction between graphene layers and the stacking issues lead to a great loss of electrochemically active surface area, damaging the performance of graphene electrodes. Developing 3D graphene architectures that are constructed of graphene sheet subunits is an effective strategy to solve this problem. The graphene architectures can be directly utilized as binder-free electrodes for energy storage devices. Furthermore, they can be used as a matrix to support active materials and further improve their electrochemical performance. Here, recent advances in synthesizing 3D graphene architectures and their composites as well as their application in different energy storage devices, including various battery systems and supercapacitors are reviewed. In addition, their challenges for application at the current stage are discussed and future development prospects are indicated.

Disciplines

Engineering | Physical Sciences and Mathematics

Publication Details

Wang, Z., Gao, H., Zhang, Q., Liu, Y., Chen, J. & Guo, Z. (2019). Recent Advances in 3D Graphene Architectures and Their Composites for Energy Storage Applications. Small, 15 (3), 1803858-1-1803858-21.

Authors

Zhijie Wang, Hong Gao, Qing Zhang, Yuqing Liu, Jun Chen, and Zaiping Guo

WILEY-VCH

DOI: 10.1002/ ((please add manuscript number))
Article type: Review

Recent Advances in Three-Dimensional Graphene Architectures and Their Composites for Energy Storage Applications

Zhijie Wang, Hong Gao, Qing Zhang, Yuqing Liu, Jun Chen* and Zaiping Guo*

Zhijie Wang, Dr. Hong Gao, Qing Zhang, Prof. Zaiping Guo
Institute for Superconducting and Electronic Materials (ISEM), Australian Institute for Innovative Materials (AIIM), University of Wollongong, Wollongong, NSW 2522, Australia
E-mail: zguo@uow.edu.au
Dr. Yuqing Liu, Prof. Jun Chen
ARC Centre of Excellence for Electromaterials Science, Intelligent Polymer Research Institute (IPRI), Australian Institute of Innovative Materials (AIIM), University of Wollongong, Wollongong, NSW 2522, Australia
Email: junc@uow.edu.au
Prof. Zaiping Guo
School of Mechanical, Materials, Mechatronic, and Biomedical Engineering, Faculty of Engineering & Information Sciences, University of Wollongong, NSW 2522, Australia
E-mail: zguo@uow.edu.au

Keywords: 3D graphene architectures, hybrid structures, electrodes, energy storage

Abstract: Graphene has been widely applied as an electrode material in the energy storage fields. The strong π-π interaction between graphene layers, however, and the stacking issues lead to a great loss of electrochemically active surface area, damaging the performance of graphene electrodes. Developing three-dimensional (3D) graphene architectures that constructed of graphene sheet subunits is an effective strategy to solve this problem. The graphene architectures can be directly utilized as binder-free electrodes for energy storage devices. Furthermore, they can be used as a matrix to support active materials and further improve their electrochemical performance. In this paper, we reviewed recent advances in synthesizing 3D graphene architectures and their composites, as well as their application in different energy storage devices, including various battery systems and supercapacitors. In addition, their challenges for application at the current stage are discussed, and future development prospects are indicated.

1. Introduction

Graphene has attracted tremendous attention since it was isolated from graphite in 2004,[1] due to its large specific surface area (SSA), superior mechanical properties, high electrical conductivity, etc. The phenomenon of aggregation and overlaying of graphene sheets induces great loss of accessible surface, however, and a relatively low electrochemically active SSA in real applications. To exhibit its excellent performance in bulk and promote its potential for practical applications, it is necessary to assemble individual graphene sheets into three-dimensional (3D) architectures.[2-4] The widely reported 3D graphene architectures (3DGAs) not only possess structural advantages and unique properties that are inherited from the graphene sheet subunits, but are also endowed with higher surface utilization and stronger operability,[5,6] The 3DGAs include graphene aerogels, graphene foams, graphene networks, and so on. Compared with other 3D carbon architectures like carbon aerogels, the 3DGAs would have larger specific surface area, advanced porous structure, better electrical conductivity and integrality as the graphene sheet subunits are ultrathin, thus giving rise to more active sites and shorter ion diffusion channels. Therefore, 3DGAs are more promising in practical applications. 3DGAs can be prepared by chemical vapor deposition (CVD) methods.[7,8] To reduce the cost, the facile and versatile graphene oxide (GO)-based chemical synthesis methods have become the most common strategies. In addition to these strategies, 3D printing technology has been applied to prepared 3DGAs in recent years.

The unique properties of 3DGAs have attracted much attention in diverse areas, such as electronics, electrochemical energy storage and conversion, sensing, biomedical engineering, and so on.[5,6,9,10] The intriguing interconnected porous macrostructures give 3DGAs high electrical conductivity, superior structural stability, and rapid diffusion channels for ions. The large electrochemically effective surface area of 3DGAs provides abundant active sites for ion storage. All of these merits allow 3DGAs to be intensively applied in energy storage applications as binder-free electrodes. What is more, 3DGAs can serve as a monolithic matrix

to support different kinds of electrochemically active materials as electrodes for energy storage devices. In this regard, recent advances in 3DGA-based electrodes have been focused on combining one or more active materials to synthesize functional hybrids with excellent electrochemical properties. Notably, in order to further improve the overall structural stability and electrochemical performance of 3DGAs, various efforts have been made, including (i) designing controllable mesoporous or micropores in the 3DGAs structure to improve the efficiency of mass transport and charge transfer;[11] (ii) decorating graphene layers with additional carbonaceous materials to enhance their overall conductivity and stabilize the 3D interconnected configuration;[12,13] (iii) enriching defects in the 3DGA framework through heteroatom doping to increase the electrochemically active sites;[14] and (iv) combining conductive polymer with 3DGAs to effectively suppress the shuttle effect in lithium-sulfur (Li-S) batteries, increase the specific capacity of supercapacitors, etc..[15] The functionalized 3DGAs combined with the electrochemically active materials could integrate the benefits of each component, thereby improving the specific performance in corresponding applications.

In this paper, we firstly summarized the recent advances in the construction strategies for 3DGAs. Then, we reviewed the applications of 3DGAs and 3DGA-based composite materials in various energy storage devices, including (i) lithium-ion batteries (LIBs) and sodium-ion batteries (SIBs); (ii) Li-S batteries; (iii) lithium metal batteries; (iv) other battery systems like Li-O_2 batteries; and (v) electrochemical supercapacitors. By making systemically summary and comparison, we concluded the achievement and challenges of 3DGAs and their composites in these areas, and the likely future developments are also discussed.

2. Synthesis of 3DGAs

Graphene exists in form of one-atom-thick and closely packed two-dimensional (2D) sp^2-bonded carbon sheets. It is challenging to directly assemble graphene into various 3D microstructures due to the serious re-stacking problem of individual graphene sheets.[16,17] A straightforward method to prepare 3D porous graphene is to grow graphene on a porous metal

template (*e.g.* Ni foam) via CVD methods. In recent years, 3DGAs are increasingly prepared from a suspension of graphene oxide (GO), which is the oxidized derivative of graphene. GO has the amphiphilic property, and it is negatively charged and has rich functional groups in its surface, all of which make it an ideal building block for constructing different microstructures.[17-20] Furthermore, the diverse GO-based fabrication strategies have the ability to create 3D hierarchical graphene-based architectures with tailored morphologies, which is of tremendous interest due to the significance of the corresponding structures for promoting the performance required in specific applications. GO suspension based strategies include the gelation of GO in suspension, GO reduction-induced self-assembly of graphene, the template-assisted assembly method, etc.[21-23] The 3D printing method has also been applied to prepare 3DGAs in these years.

2.1. CVD methods

The CVD method makes it possible to synthesize 3DGAs with controlled layer and morphologies. In this method, metal substrates (such as Ni foam) are normally used as catalyst. At high temperature, organic precursor (such as CH_4, C_2H_6, and glucose) vapors undergo pyrolysis and carbon deposition on the substrate, and after the substrate removal process, 3DGAs with different structures and properties can be achieved.[24-26]

Chen et al. were the first to use the CVD method to develop 3D graphene foam (GF).[27] They used Ni foam as the substrate and catalyst, CH_4 as the carbon precursor, and an Ar/H_2 mixture as the carrier gas. The CH_4 was deposited at 1000 °C under ambient pressure, and then 3-layered graphene films were precipitated on the surface of the Ni foam. To protect the graphene foam, a thin layer of poly(methyl methacrylate) (PMMA) was coated on the surface of the graphene-Ni composite, and after that, the Ni substrate was etched with hot HCl or $FeCl_3$ solution. The obtained GF can be used to make composite (for example GF-polydimethylsiloxane (GF-PDMS)) for other applications. Inheriting the 3D interconnected network of Ni foam, the 3D GF has a continuous and interconnected structure, in which

graphene nanosheets are in direct contact with each other without any breaks. Cao et al. has done a similar work for the application of supercapacitor by switch the carbon source to ethanol.[28]

2.2. GO-based chemical synthesis methods

2.2.1 Gelation of GO in suspension

GO can form a stable dispersion in water due to its various hydrophilic oxygenated functional groups.[29] The gelation of GO can be achieved either by disrupting the dispersion balance or adding a cross-linker. Increasing the bonding force or weakening the repulsion force is an effective way to disrupt the dispersion balance. A facile method to achieve GO gelation is decreasing the pH value of the GO solvent, which can weaken the electrostatic repulsion and simultaneously enhance the hydrogen bonding force (due to the protonation of carboxyl groups).[30] Additionally, introducing salt ions to change the interactions in the GO solution is another option to achieve controlled destabilization of the GO dispersion and then form GO gels.[31,32]

The cross-linkage of GO sheets is another effective method, for which various cross-linkers utilizing different reaction mechanisms have been intensively studied. For examples, several polymers (such as polyvinyl acetate (PVA), polyethylene oxide (PEO), hydroxypropylcellulose (HPC), polyvinylpyrrolidone (PVP), ethylenediamine (EDA), polyamines (PA), etc.) have been used to generate hydrogen bonds between GO sheets and form GO gels.[33-36] Additionally, cationic molecules containing quaternary ammonium salts, such as cetyltrimethyl-ammonium bromide (CTAB) and tetramethylammonium chloride (TMAC), could promote long-range electrostatic attraction towards the anionic charged GO sheets.[38] The existence of high density amine groups in polyethyleneimine (PEI) chains is conducive to protonation on the polymer, leading to both hydrogen bonding and electrostatic attraction between PEI and the GO sheets.[36] Some other cross-linkers, such as polyamines, ethylenediamine, thiourea, and pyrrole, could react with the functional groups on GO to form

covalent bonding, resulting in improved mechanical strength. For instance, cross-linkers containing amines can easily react with the epoxide, carboxyl, and hydroxyl groups on GO at high temperature.[37] Interestingly, some nanoparticles, such as $KMnO_4$, can act as cross-linkers as well. The strongly oxidative $KMnO_4$ reacts with carbon atoms on reduced graphene oxide (rGO) and generates defects with dangling bonds, which enable the reduced MnO_2 to cling to and form an interconnected network with rGO sheets.[38] Apart from the above mentioned cross-linkers, metal ions with multivalent states (e.g., Ca^{2+}, Mg^{2+}, Cu^{2+}, Pb^{2+}, Cr^{3+}, Fe^{3+}) could also interact with individual GO sheets via bonding forces and promote the gelation of GO.[39] Biomacromolecules can interact through π-π stacking, electrostatic interaction, and hydrogen bonds with GO sheets.[40]

2.2.2. GO-based template-assisted assembly

Apart from the above-mentioned strategies, utilizing various sacrificial templates is another approach to prepare 3DGAs, in which the size, uniformity, and shape of the whole 3DGA framework can be precisely controlled.[41] Along with the traditional templates, such as Ni foam, some other different templates were utilized to achieve the 3D structures.[42] Zhai et al. fabricated a 3D graphene hollow (3DGH) structure via the assistant of Ni foam template.[43] Firstly, Ni foam was immersed in GO solution at 160 °C for 12 h to deposit GO on the Ni skeleton. After the vacuum-drying and template removal process, the obtained product was reduced to graphene at high temperature (900 °C). The 3DGH had a low mass density of 0.82 mg cm^{-2} and certain degree of flexibility (**Figure 1a**), with its construction based on a hollow graphene skeleton ~ 100 μm in diameter and several nanometers in thickness (**Figure 1b and 1c**). Due to these structural advantages, the 3DGHs can be used as active materials or current collectors to support electrode materials for energy storage applications.

Ice crystals can act as solid templates to shape the building blocks and achieve the desired porous structure. Qiu et al. prepared an ultralight and superelastic cellular structured graphene monolith (**Figure 1d-f**) by freeze-casting of a partially reduced GO suspension.[44] The pre-

reduced GO was squeezed and forced to align along the moving solidification front, yielding a highly ordered cellular structure. Therefore, the ice-template technique is a facile and straightforward self-assembly strategy to obtain porous microstructures. Some other techniques (such as the spray-drying method, the boiling assisted method, the breath-figure self-assembly strategy, etc.) have been applied to realize 3DGAs.[45,46] All of these fascinating efforts have paved the way to exploring the fabrication and application of 3DGAs.

Normally, to convert the obtained 3D GO architectures to 3DGAs, the subsequent reduction process is essential. The most common strategy is using reduction agents such as hydrazine, ascorbic acid, etc.. Due to the low temperature of these reduction reaction, the prepared graphene foam have low C/O ratio, and unsatisfactory electric conductivity and mechanical properties.[47,48] Thermal reduction at high temperature could improve the conductivity, but it may sacrifice the mechanical strength of the 3DGAs. In order to solve this problem, Tang et al. reported a magnesiothermic reaction at 700 °C to reduce freeze-dried GO gel, and achieved an rGO foam with high conductivity of 27.7 $S \cdot m^{-1}$ at 3.6 $mg \cdot cm^{-3}$ and good mechanical performance (**Figure 1g**).[49]

2.3.3. GO reduction-induced self-assembly of graphene

3D porous graphene can also be prepared from GO by a solution-based reduction process, where the partial removal of oxygen functional groups can induce the self-assembly of graphene sheets into a 3D network.[50] The hydrothermal method is the most common strategy for the reduction of GO to construct graphene-based hydrogels. Here, water acts as the reducing agent, and the mechanism behind the reduction process is similar to that for the H^+-catalysed dehydration of alcohol.[51] For instance, Xu et al. reported the self-assembly of a 3D graphene hydrogel via a hydrothermal process and found that, when the concentration of the GO dispersion went over a certain amount, the self-assembly of graphene would take place.[50] The hydrothermal method also involves high temperature and high pressure, however, which limits possibilities for large-scale application. Alternatively, the chemical reduction strategy

can be conducted under mild reducing conditions (< 100 °C and normal atmosphere) by adopting mild reduction agents, such as sodium ascorbate, $NaHSO_3$, Na_2S, ascorbic acid, hydroquinone, hydrogen iodide (HI), etc. For example, Chen at al. fabricated a 3DGAs under mild chemical reduction (95°C, atmospheric pressure) with various reducing agents.[52] They also found that the gel synthesized using HI and $NaHSO_3$ had better electrical conductivity. Worsley et al. reported that, with the assistance of NH_4OH, even at 85 °C, the gelation of GO still could be observed.[53] Goldstein et al. demonstrated that the physical changes in GO bond formation were accompanied by the removal of oxygen functional groups, with the partial re-formation of the sp^2 network during the assembly process for the 3D structure.[54] Its simplicity and scalability have made the chemical reduction route a facile and effective way to prepare 3DGAs on a large-scale.

2.2.4. Factors influencing the synthesis

The formation of 3D porous structures will be greatly influenced by various conditions.[55] According to the choice of 3DGA formation method and the relevant parameters, researchers can tailor the fabrication process and obtain specified 3D porous architectures to satisfy the needs of the corresponding application.

It is well established that the pore morphologies have affinities to some physical properties of the 3D architectures.[56-58] For instance, the mechanical stability of the as-prepared 3DGAs is determined by the interconnectivity, degree of crosslinking, etc.. Meanwhile, some properties, such as the pore size distribution and density of the 3DGAs, can be tailored by controlling the synthesis parameters.[52,57] Xu et al. studied the assembly behavior of 3DGAs by adjusting the concentration of the initial GO and the reaction time of the hydrothermal process.[50] The results demonstrated that the concentration of GO could affect the size and strength of the 3DGAs, while the reduction time could be used to tailor the electrical conductivity and size of the resultant 3DGA. The density and pore size distribution of the 3DGAs were also determined by the size of the selected GO precursors. Compared to the

large-size GO nanosheets, smaller ones would result in a higher 3DGA density and smaller pore size. Some other properties, such as the pore wall thickness of a hydrogel would be affected by introducing site specific cross-linkers.[13] The orientation of the pores in the 3D construction could be controlled by adjusting the orientation of the 2D GO precursors. The orientation-controlled 3DGAs could exhibit anisotropic conductivity and acoustic vibrations that were guided in desired directions. After the formation of the graphene hydrogel, the drying method could help to adjust the volume and density of the porous framework.[57] For example, Han et al. obtained graphene aerogel by soaking graphene hydrogel in ammonia solution, which can control the density as well as volume of the GA through adjusting the concentration during the freeze-drying process (**Figure 1h**).[57]

2.3. 3D Printing methods

Apart from these methods, 3D printing is another effective strategy to prepare 3DGAs. The 3DGAs which are synthesized by 3D printing methods can achieve higher mass loading and other tailored properties for energy storage applications.[59-63] Zhu et al. reported 3D periodic graphene aerogel architectures that were prepared via 3D printing methods. These aerogels are lightweight, and have high conductivity and supercompressibility (up to 90 % compressive strain) (**Figure 2**).[64] The GO inks were prepared by combining highly-concentrated GO suspensions with silica powder to form a homogenous, highly viscous and thixotropic ink for printing. $(NH_4)_2CO_3$ or sol-gel chemicals (as with resorcinol-formaldehyde (R-F) solution) were added into the inks to gelate the concentrated GO suspensions. Then the inks were transferred into a spring barrel, and extruded through a small-size nozzle to pattern 3D architectures in an isooctane bath (to avoid drying of the inks in air). Afterwards, the printed microlattice architecture was supercritically dried to remove the solution before being heat treated at 1050 °C under N_2 atmosphere for carbonization, while, the GO was reduced to graphene at high temperature. Finally, the silica powder was washed with hydrogen fluoride (HF) solution. The prepared 3D cubic graphene microlattices were designed with an in-plane

center-to-center filament space of 1mm and a diameter of 0.25 mm, resulting in a space-to-diameter ratio of 4. By adjusting the filament space and diameter, the densities of the printed 3DGAs could be controlled. The using of R-F solution led to a more open and less cross-linked network compared with gelation methods based on gelation without R-F solution. The mechanical strength of the 3D printed graphene architectures showed an order of magnitude improvement compared to bulk graphene. By using similar strategy and adding graphene nanoplatelets (GNP) into GO suspension to reduce the electric resistance in the final products, Zhu et al further developed 3D printed graphene composite aerogels (GCA), which were lightweight and highly conductive, for high-energy-density supercapacitors.[65]

The 3D-printing methods could be used to prepare 3DGAs with controllable microstructures and morphologies on a large scale. The key challenges in this method are, (i) developing printable GO-based or graphene-based inks with suitable viscous and thixotropic properties; (ii) maintaining the intrinsic properties of single graphene sheets, such as large surface area, and excellent mechanical and electrical performance.

For a short summary, CVD is a straightforward method to synthesize highly-conductive 3DGAs with loose structure and low density. Nevertheless, considering the high-cost and sophisticated process involved in rigorously controlling the deposition temperature and pressure, the use of a carbon-based gas source, and the additional etching process for the metal template, this approach is not practical for large-scale preparation of 3DGAs. The GO-based chemical synthesis methods are more facile and versatile. In terms of the gelation of GO in suspension methods, GO can be easily gelated by disrupting the dispersion balance or adding a cross-linker, although a subsequent reduction process is required. As for the GO-based template-assisted method, it is useful to design the structure of the 3DGAs by controlling the shape of the templates, although the template removal process is needed. Without an individual reduction process, the GO reduction-induced self-assembly of graphene method is more convenient. Finally, the 3D-printing method, it is facile to fabricate 3DGAs

with different spatial structures, and 3D printing would have advantages to prepare 3DGAs on a large scale.

3. 3DGAs as electrode materials for batteries

3DGAs have been synthesised and are widely used as electrode materials for battery systems, such as LIBs and SIBs.[66-68] The 3D design helps to reduce the loss of electrochemically active surface area for energy storage, and the porous structure also facilitates the diffusion of electrolyte ions in the electrodes. As a result, 3DGAs exhibit superior electrochemical properties.[69-72] More importantly, because of the nature of high electrical conductivity and integrity, 3DGAs could be excellent self-supported electrodes.

The typical discharge-charge curves reveal that the lithiation behaviour of graphene combines the features of both graphitic carbon and hard carbon (**Figure 3a**).[73] The capacity in the region higher than 0.5 V is related to the faradic capacitance of the graphene surface and edge sites, while the capacity in the low-voltage region below 0.5 V can be assigned to Li^+ binding on the basal planes of graphene layers. It is worth noting that there is an irreversible voltage slope at ~ 1.0-0.6 V in the first discharge process, which should be attributed to the formation of the solid electrolyte interphase (SEI) on the huge surface area of graphene (**Figure 3a**).[73] Similar to its behaviour in LIBs, the SEI forms at ~ 0.5 V with high irreversible capacity loss when graphene is used as anode for SIBs (**Figure 3b**).[74] No obvious voltage plateaus can be observed in the following charge-discharge cycles. The 3DGAs delivered the same lithiation and sodiation behaviours as individual graphene nanosheets with enhanced electrochemical performance. The interconnected structure of 3DGAs effectively improves their Li^+/Na^+ storage performance. Zuo et al. fabricated a 3D graphene foam with large-scale continuity and used it as a binder-free anode for LIBs (**Figure 4a**).[75] This 3D graphene anode had interlayer pores and a high SSA of 835 $m^2\ g^{-1}$ (**Figure 4b**). Based on its interconnected porous structure, it delivered a discharge capacity and a charge capacity of 1519 mAh g^{-1} and 932 mAh g^{-1} respectively, with an initial Coulombic

efficiency (ICE) of 61.3%. Even at the high discharge rate of 2 A g^{-1}, the capacity still reached 342 mAh g^{-1} (**Figure 4c**).[75] Zhang et al. used hydrothermal, freeze-drying, and annealing methods to synthesize a N-doped 3D free-standing rGO aerogel (**Figure 4d**).[76] The 3D porous structure could provide sufficient space for Na^+ storage and enable fast and reversible Na^+ insertion. The doped N heteroatoms, especially pyrrolic N and pyridinic N, could create more electrochemically active sites for Na^+ storage. When applied as SIB anode, it exhibited a stable capacity of 287.9 mAh g^{-1} at 100 mA g^{-1}, superior to that of rGO sheets (**Figure 4e**).[76]

Although the 3DGAs showed high Na^+/Li^+ storage capabilities, the large capacity loss in the first cycle and low ICE are worth attention (**Table 1**). This phenomenon was more serious in SIBs. In addition, there were no obvious voltage plateaus in the discharge-charge process when GAs were used as anodes for LIBs or SIBs. These drawbacks have greatly hindered the practical application of 3DGAs. So, addressing these problems is of major significance. Rational design of the SSA and pore size distribution of 3DGAs would be helpful.

Moreover, the 3DGAs possessed low density due to their porous structure, which certainly reduced the volumetric energy density of the electrodes. Continuous efforts have been made to develop high-volumetric-density 3D graphene electrodes. For example, Zhang et al. constructed a high-density porous graphene macrofoam (HPGM) through a 3D densification method for high-density SIBs (**Figure 5a-c**).[77] To be specific, the HPGM was prepared by drying graphene hydrogel at 80 °C in an air-circulating oven. The obtained HPGM had a density of 1.04 g cm^{-3}, much higher than that of porous graphene foam (PGM) (0.32 g cm^{-3}) that was prepared by freeze-drying graphene hydrogel. Xu et al. reported a solvent-exchange approach to prepare solvated graphene frameworks (SGFs) by using graphene hydrogel as precursor (**Figure 5d**).[78] The obtained SGFs were pressed and used as anode for LIBs (**Figure 5e**). In this anode, the graphene layers were stacked together tightly (**Figure 5f**), leading to a high packing capacity of 0.65 g cm^{-3}. It delivered stable Li^+ storage capacity as

high as ~ 1360 mAh g^{-1} (**Figure 5g**). When the discharge current density was increased to 5 A g^{-1}, the capacity was still over 300 mAh g^{-1} (**Figure 5h** and **5i**). The volumetric capacity was calculated to be as high as 487 mAh cm^{-3} at 1 A g^{-1}.

In consideration of its low ICE, lack of voltage plateaus, and low density, it is reasonable to conclude that 3DGAs are not the best electrode candidates for batteries. Alternatively, the porosity advantage of 3DGAs can be used to support active materials for different battery systems. Constructing 3D composites of graphene and electrochemically active materials would be more promising for energy storage applications.

4. 3DGAs supporting active materials as composite electrodes for batteries

3DGAs usually serve as an excellent support matrix for electrochemically active materials to alleviate their mechanical stress that is caused by volume changes during cycling. In addition, 3DGAs are able to improve the electrical conductivity of these active materials. Furthermore, the 3D interconnected porous structure promotes access of electrolyte ions into electrodes. The 3D framework can also stabilize the structure of the overall electrodes during cycling. Therefore, introducing 3DGAs as a supporting matrix is an effective strategy to improve the electrochemical performance of various materials, including their discharge/charge capacity, cycling stability, and rate performance.[44,79-81]

4.1. 3DGA-based composite electrodes for LIBs

To date, various strategies have been applied to develop 3DGA-based electrode materials for LIBs.[82-88] For instance, some research groups have employed simple one-pot hydrothermal methods to prepare composites of 3D-structured active materials with 3DGAs.[83,84,87] Compared with bare active materials, their counterparts in a 3DGA matrix exhibited improved cycling performance and rate capability. In addition, a facile centrifugation method was introduced to fabricate a 3DGA-based composite hybrid, in which metal-organic framework (MOF)-derived porous Fe_2O_3 was encapsulated in a graphene

aerogel framework (3DG@Fe_3O_2).[89] The porous Fe_2O_3, which has poor electrical conductivity and mechanical strength, was reinforced by the graphene aerogel matrix. This kind of structure provided Fe_2O_3 with an interpenetrating conductive network, enough buffer space to accommodate the stress, and robust structural stability during cycling. Lee at al. fabricated a few layer MoS_2-anchored graphene aerogel paper (MGAP) to form a composite to act as a free-standing LIB anode material, in which graphene paper served as the conductive matrix for the MoS_2 sheets and as a free-standing support.[90] Gao et al. developed a 3D V_2O_5@N-doepd graphene composite aerogel (V_2O_5@3DNG) via a one-step hydrothermal strategy, in which V_2O_5 particles were confined in a graphene framework (**Figure 6a** and **6b**).[91] Benefiting from the graphene aerogel matrix, when applied as cathode for LIBs, the composite aerogel delivered enhanced electrochemical performance.

Combinations of 3DGAs with carbonaceous materials have proved to be effective for further improving the electrochemical performance of 3DGA-based composite electrodes.[10,11,92] To construct a stable 3D carbonaceous interaction matrix, the most typical approach is decorating the graphene framework with carbonaceous materials as additives. For example, Wei et al. fabricated a composite electrode in which Fe_3O_4 nanospheres prewrapped in graphene sheets (GS) were confined in a 3D graphene framework (Fe_3O_4@GS/GF).[93] The double-shelled graphene protected the Fe_3O_4 nanospheres from aggregation, further alleviated the volume expansion, and improved the overall conductivity (**Figure 6c**). Similarly, a 3D composite was reported that consisted of Si nanoparticles prewrapped in graphene sheets and embedded into the backbone of a 3D graphene honeycomb.[94] The dual graphene coats could not only protect the Si nanoparticles from structural collapse during volume changes, but also allowed stable SEI formation to take place on the graphene rather than on the Si nanoparticles. The extra carbonaceous materials could link the active materials with the graphene framework, increasing the structural stability of the composite electrode.

Chemical functionalization of 3DGAs, such as by heteroatom doping, could potentially

allow highly reactive sites to exist inside the structure. The doped 3DGAs with abundant defect sites has advantages in terms of the dispersion of active materials, improving the binding force, and further promoting the lithium storage capability and the transportation rate of Li ions.[95] Thus, the doped 3DGAs are superior in combination with active materials for energy storage application.[96,97] For instance, Han et al. reported a composite for LIBs in which Co_3O_4 particles were uniformly embedded in a N-doped graphene network (Co_3O_4@NGN).[14] The electrode showed enhanced capacity of 676 mA h g^{-1} at 1 A g^{-1} after 400 cycles. Furthermore, the co-existence of extra carbonaceous materials and heteroatom doping in the 3DGA framework could combine the benefits of each component, and their synergistic effects could further improve the energy storage performance of 3DGA-based composite electrodes. In this regard, a 3D porous carbon coated MoS_2/N-doped graphene composite (C-MoS_2/N-G) was reported for LIB anode.[98] The coated carbon and doped N heteroatoms could increase the density of active sites in the graphene framework, while simultaneously modulating the electronic structure of the whole composite and further enhancing its Li^+ storage capability.

4.2. 3DGA-based composite electrodes for SIBs

Alloy-based anodes, such as Sn and P, are popular SIB anode materials due to their high theoretical capacity.[99,100] Nevertheless, they suffer from severe volume changes during sodiation/de-sodiation cycles, leading to poor electrochemical performance. In order to solve this problem, alloy-type anodes were made into composites with 3DGAs to construct hybrid structures for SIB anodes.[101,102] For example, in order to further improve the SIB performance of red P, Gao et al. constructed a 3D integrated carbon/red P/graphene aerogel composite (C@P/GA) (**Figure 7**).[103] A vapor-redistribution strategy was adopted to disperse the red P nanoparticles uniformly within the 3D graphene-based architecture. In the obtained C@P/GA architecture, red P nanoparticles with a size of 10-20 nm were uniformly encapsulated in the crumpled matrix and covered by carbon and graphene sheets. With the

benefits of this advanced structure, C@P/GA delivered excellent electrochemical performance. Even at 1 C (2.6 A g^{-1}), the sodium storage capacity was still higher than 720 mAh g^{-1}. The excellent SIB performance of the C@P/GA architecture was attributed to its unique design. During the sodiation/de-sodiation process ($P + 3Na^+ + 3e^- \leftrightarrow Na_3P$), P nanoparticles were confined in the C@GA matrix, increasing the interfacial contact between P and the carbon framework, as well as accommodating the volume changes of red P (**Figure 7**). Similar to red P, the volume expansion of Sn during sodiation is one of the main obstacles to its practical application.[104] By constructing 3D graphene/Sn composites, this problem can be effectively addressed. In this regards, Pan et al. synthesized a Sn/3D graphene nanosheet (Sn/GS) composite, in which small-size Sn particles (~ 10 nm) were uniformly distributed within the 3DGAs.[104] The obtained Sn/GS composite was applied as free-standing anode for SIBs, and thanks to its structural advantages, it delivered much better electrochemical performance than pure Sn nanoparticles.

Some conversion type anodes also suffer from serious volume changes during the sodiation process, such as metal oxides (SnO_2, Sb_2O_3, Fe_3O_4, Co_3O_4, etc.)[105-109] and metal sulfides (MoS_2, Sb_2S_5, SnS, etc.)[110-112]. In addition, their poor intrinsic conductivity negatively affect their electrochemical performance. These drawbacks lead to capacity fading and poor rate performance. Distributing the conversion type anode materials into 3DGAs can solve these problems and achieve better electrochemical performance. For example, Li et al. constructed a SnO_2-graphene dual aerogel and studied its sodium storage properties (**Figure 8a**).[109] In this composite, SnO_2 crystallites ~ 5 nm in size were conformably blended with distorted graphene planes (**Figure 8b**). When applied as SIB anode, the graphene-SnO_2 aerogel delivered an enhanced capacity of 221 mAh g^{-1} (**Figure 8c**). Hu et al. supported MoS_2 with 3D graphene and used the graphene/MoS_2 composite as anode for SIBs. In the obtained composite, few layered MoS_2 nanosheets were uniformly combined with graphene aerogel, forming a 3D porous architecture (**Figure 8d** and **8e**).[113] Benefiting from these structural

advantages, the composite delivered a discharge capacity of 1145 mAh g^{-1} after 100 cycles at 0.1 A g^{-1}, much better than the performance of pure MoS_2 (**Figure 8f**). Similarly, 3D aerogels of graphene-CNT-WS_2 (**Figure 8g**), where CNT is carbon nanotube,[114] graphene-Sb_2S_5 (**Figure 8h**),[111] and graphene-Bi_2S_3 (**Figure 8i**)[115] were also developed, and the results also proved that the combination with 3DGAs could help to increase the capacity retention and rate capabilities of conversion type electrode materials.

To summarize, the 3DGA matrixes successfully improved the energy storage performance of the electrochemically active materials. The superior performance of 3DGA-based composite materials originates from their porous structure, enhanced electrical conductivity, and overall structural stability. Most of the 3DGA-based composite structures were utilized as anodes for LIBs/SIBs. In these composite anodes, both the 3DGAs and the active materials contributed to the Li^+/Na^+ storage capacity. Because of this, the composite electrodes exhibited the disadvantages of both components. Normally, the composite anodes delivered a low ICE and relatively high voltage plateaus, which make them imperfect candidates for industrial use (**Table 1**). In addition, at the current stage, the mass loading of active materials on 3DGA substrate is not sufficient for practical application. Optimization of the structure of the 3DGA matrix would be an effective way to solve these problems. In addition, choosing better active materials which have higher ICE and appropriate voltage plateaus could also be useful to boost the application of 3DGA-based composite anodes.

4.3. 3DGA supporting cathodes for Li-S batteries

Li-S batteries are regarded as promising power sources, due to their ultrahigh theoretical capacity of 1675 mAh g^{-1} and energy density of 2576 Wh kg^{-1}.[116-119] Nevertheless, the intrinsic insulating property of S and the shuttle effects of the intermediate polysulfides (Li_2S_x, $4 \leq x \leq 8$) greatly shorten their life-span and damage their electrochemical performance.[111-114] Porous carbon nanomaterials, such as the ordered carbon CMK-3, have been successfully utilized for accommodating the S cathode and solving these problems.[120] Among them,

3DGAs would be classical representatives. The intrinsic conductivity of 3DGAs improves the electrical conductivity of S. In addition, the porous structure helps to enhance the mass loading of S and ensure good infiltration of electrolyte.[121] More importantly, due to their strong capability to absorb electrolyte, the nanostructure of 3DGAs is able to suppress the migration of polysulfides, thus alleviating the shuttle effects. Therefore, 3DGAs are ideal cathode hosts for high-performance Li-S batteries. Beyond S, lithium sulfides (Li_2S) and even lithium polysulfides have also been studied as cathodes in recent years. Similarly, the construction of 3DGAs and Li_2S/lithium polysulfides composites was reported to be useful for improving the performance of Li_2S cathode.[122]

For example, Zhou et al. developed a 3D doped graphene sponge to accommodate large amounts of dissolved lithium polysulfides as cathode for Li-S batteries.[123] The freeze-dried 3D graphene sponge was cut and pressed into slices, and applied as a host to absorb lithium polysulfides without current collectors or binders (**Figure 9a** and **9b**). The composite cathode, with active materials loading as high as 4.6 mg cm^{-2}, delivered high capacity of 1200 mAh g^{-1} at 0.2 C as well as excellent capacity retention. A similar 3D binder-free rGO architecture supported S composite cathode (S-r-GO), was reported to exhibit an excellent areal capacity of 3 mAh cm^{-2} after 75 cycles.[124]

Although these improvements have been achieved, 3DGAs alone are not sufficient to prevent polysulfides from taking part in the shuttle effect. For this purpose, additional carbonaceous materials, such as carbon nanotubes (CNTs), porous carbon, and pyrrole, have been utilized to construct porous hybrids with 3DGAs.[125] This kind of architecture is able to act as a trap to capture the polysulfides and enhance the mass loading of cathodes. In addition, the micro-, meso-, and macrospores, as well as the large size pores inside the hybrids, can facilitate efficient penetration of the electrolyte and guarantee rapid transport of Li^+ ions.[126-130] In this regard, a 3D CNT/graphene-Li_2S cathode (3DCG-Li_2S) with ultra-high Li_2S loading of 81.4 wt.% was realized through hydrothermal reaction and a subsequent liquid-

infiltration-evaporation coating technique (**Figure 9c-f**).[131] The highly flexible and conductive 3D mesoporous interconnected network based on CNT/graphene provided efficient channels for electron transfer and ionic diffusion, and decreased the solubility of polysulfides in the electrolyte during cycling. As a result, the CNT/graphene-Li_2S cathode exhibited a high reversible capacity of 1123.6 mAh g^{-1} with 0.02% capacity decay per cycle, as well as a high-rate capacity of 514 mAh g^{-1} at 4 C. Another typical example is a hybrid carbon aerogel (HCA) film that was constructed from graphene sheets and CNTs, and was investigated as an interlayer between the cathode and the separator for Li-S batteries (**Figure 10a**).[132] To prepare the HCA film, a dispersion of graphene sheets and CNTs was poured into a planar aluminum foil container and then placed above liquid N_2, followed by freeze-drying. The hierarchical cross-linked networks of the HCA interlayer help to capture the soluble polysulfides, without affecting the ion diffusion speed because of its porous properties.

Since the intrinsic non-polar C-C bonding in the 3DGA host cannot offer sufficient chemisorption for polar polysulfides, additives with good absorption of polysulfides are added into 3DGAs to further restrain shuttle effects.[133-136] Polar polymers, such as polyaniline, polythiophene, and polypyrrole, have high conductivity and good compatibility with polysulfide intermediates, but they lack enough space for cathode loading. Therefore, adding conductive polymer to provide absorption sites on the graphene aerogel framework is a rational design to reach the expected target. In addition to polymers, pyrrole monomer has similar effects, along with better dispersibility in 3DGAs and better adhesion to the carbon framework. For example, a pyrrole modified graphene host has been applied for high-performance S cathode (Py-GF@S).[137] In this structure, pyrrole provided strong chemical bonding for polysulfide anchoring, and graphene aerogel served as a matrix to enhance the conductivity as well as simultaneously increasing the loading content of the S cathode. The composite cathode, with a high mass loading of ~ 6.2 mg cm^{-2}, displayed an initial specific capacity of 985.8 mA h g^{-1} and capacity retention of 81% after 100 cycles at 0.5 C.

Researchers also found that some polar materials, such as ZnO, MgO, and Li_3PS_4, were effective absorbing agents for trapping the soluble polysulfides.[1149] For example, graphene aerogel/TiO_2 composite, with S loading of 75.1 wt.%, was adopted as cathode (GA/TiO_2/S) for Li-S batteries.[138] The cathode exhibited a discharge capacity of 512 mAh g^{-1} after 250 cycles at 1 C with a capacity decay of 0.128% per cycle. The formation of chemical bonds between TiO_2 and S nanoparticles was critical for restricting the dissolution of polysulfides. Yu et al. developed an atomic layer deposition (ALD) technique to modify an ultrathin ZnO or MgO layer on the graphene aerogel-S composite skin.[139] The graphene aerogel skin and ZnO or MgO layer (ZnO/G-S or MgO/G-S) worked together as barriers to confine the polysulfides within the electrode region. Jiao et al. proposed a Li_2S@Li_3PS_4/GA composite (in which GA refer to graphene aerogel) as cathode for Li-S batteries.[140] The Li_3PS_4 coating layer could improve the conductivity of the whole electrode and provide protection for the Li_2S cathode to some extent.

To further restrain the dissolution of polysulfides, heteroatoms, such as N, S, B, and F, are doped into 3DGAs to form polar domains on the carbon framework, which can interact chemically with the polysulfides and thus alleviate the shuttle effects.[125,141,142] For instance, a porous B-doped 3DGA loaded with S was prepared for Li-S batteries. The doped B heteroatoms became chemical adsorption sites for the negative polysulfides. Compared with un-doped 3DGA/S composite, the B-doped 3DGA/S composite delivered both higher capacity and better rate capability.[143] Zhou et al. developed a Li_2S coated 3D B-doped or N-doped graphene aerogels as a self-supported cathode through a facile liquid infiltration-evaporation coating method for Li-S batteries (**Figure 10b-d**).[144] Nevertheless, the introduction of heteroatoms into the graphene-based materials would generate an energy gap between the valence and conduction bands and hinder the facile transmission of electrons. Thus, the combination of the extra conductive additive and heteroatoms in 3DGAs would be an excellent design to overcome the above-mentioned drawback.

It is worth noting that, because of their high working potential, the 3DGA hosts make a negligible capacity contribution in Li-S batteries. Despite the success of 3DGAs towards improving their electrochemical performance, the cathode loading content is not satisfactory for industrial applications. In addition, the shuttle effects of polysulfides have not been addressed well to data, and the capacity fading during cycling is still a big problem (**Table 2**). Optimization of the pore structure and increasing the pore volume of the 3DGA matrix would be helpful towards improving the cathode loading. Beyond one-element doping, dual-element doping or tri-element doping on the 3DGA framework could be useful to trap the polysulfides. Furthermore, combinations of different modification strategies, such as heteroatom doping and polar material modification, would have synergistic effects towards further improving the performance of Li-S batteries.

4.4. GAs as support for lithium metal batteries

Li metal is an ideal anode material for next-generation batteries because of its ultrahigh capacity (3860 mAh g^{-1}) and low redox potential (-3.04 V *vs.* the standard hydrogen electrode).[145] Nevertheless, the enormous volumetric changes of lithium metal anode and uncontrollable dendrite growth during plating/stripping processes are greatly impeding its practical application. To address the above issues, the key lies in regulating the Li deposition behavior and providing the necessary space to mitigate volumetric change.[146] Based on the above considerations, well-designed conductive matrices have been developed as stable hosts to mitigate volumetric change and entrap Li dendrites.[147-150] Since the weight of the conductive matrix dominates the real energy density of composite electrodes, carbon-based porous matrices, typically 3DGAs, show irreplaceable advantages compared with metallic matrices.[147]

Jin et al. fabricated a 3DGA with an interconnected microtube structure and applied it as host for Li metal anode.[151] The 3DGA was covalently connected, exhibiting the desired mechanical strength and stability during cycling (**Figure 11a-c**). With the advanced porous

architecture of the 3DGA, the thickness changes of Li metal electrode were controlled within an acceptable level at around 9% during plating/stripping processes. The Li metal anode with the 3DGA as host demonstrated a long lifespan of up to 3000 hours, even with high cycling capacity of 10 mAh cm^{-2} and high cycling current density of 1 mA cm^{-2}. Its reversible gravimetric capacity was calculated to be as high as 913 mAh g^{-1}. Lin et al. proposed a 3D layered Li-rGO composite electrode prepared by a subtle "spark" reaction.[152] When densely stacked GO films came into contact with molten Li, volatile residual water and surface functional groups of GO were released under the reducing conditions, and the generated gas pressure expanded the films into a porous structure with uniform nanogaps. The formation of the 3D structure could overcome the stacking problem of rGO films and also provide interlayer space to absorb molten Li (**Figure 11d**). Thanks to the lightweight rGO matrix, which only took up 7 wt.%, the as-obtained Li-rGO composite electrode delivered capacity as high as ~ 3390 mAh g^{-1}. The porous rGO played an important role in maintaining the dimensional stability of the composite electrode, and only ~ 20% thickness fluctuation was observed during Li plating and stripping processes. Zhao et al. introduced a free-standing Li_xSi/graphene foil to replace Li metal anode.[153] The Li_xSi nanoparticles were synthesized via heating Li metal and Si nanoparticles in Ar atmosphere. Fully expanded Li_xSi nanoparticles were mixed with graphene sheets and then casted onto a free-standing foil. The densely packed Li_xSi nanoparticles were confined in 3D graphene networking to avoid contact with gas molecules (**Figure 11e**). Consequently, the Li_xSi/graphene foil exhibited excellent air stability, which is a significant improvement in terms of enhancing safety in use and simplifying the requirements on the industrial battery fabrication environment. The specific capacity of the obtained electrode was ~1600 mAh g^{-1}. When the electrode was paired with sulfur and V_2O_5 cathodes, the energy densities of the full cells reached 490 Wh kg^{-1} and 510 Wh kg^{-1}, respectively.

3DGAs are non-wieldable, however, which may become an engineering problem in

practical production. How to connect the host materials with a thin metallic current collector has hardly been reported, and it needs further exploration.

4.5. GA-based composite electrodes for other batteries

Selenium (Se) has a similar lithiation/de-lithiation mechanism and a comparable theoretical volumetric capacity to S. As in Li-S batteries, 3DGAs can also act as a support matrix to improve the electrochemical performance of Se cathodes. He et al. proposed a 3D graphene-CNT@Se composite aerogel as cathode, which was prepared with CNT/Se sandwiched between graphene nanosheets.[154] The obtained composite cathode delivered improved capacity and enhanced rate capability compared to Se.

Apart from the above battery systems, 3DGA-based composites can also be used in metal-O_2 batteries and metal-air batteries. For example, Zhou et al. reported Ru-particle modified graphene aerogels (Ru-GAs) that were directly used as a free-standing cathode for the Li-O_2 battery, which delivered a high capacity of 12000 mAh g^{-1} and excellent cycling performance.[155] Sun et al. reported an Ag nanowire-graphene aerogel composite for the Zn-air battery that was synthesized by a facile method involving in-situ integration of silver nanowires during gelation of the GO sheets. The composite exhibited ultrahigh discharge rates of up to 300 mA cm^{-2}.[156] In this composite, the hierarchical porous structure facilitated electrolyte infiltration and gas diffusion, and the 3D interconnected structures provided easy electron transfer paths; the high SSA offered abundant active sites for electrochemical reaction, and the large pore volume was able to accommodate the discharge products.

5. 3DGAs and 3DGA-based composites for supercapacitors

Electrochemical supercapacitors have attracted wide research interest due to their fast discharge-charge capacities.[157] The performance of supercapacitor electrodes is determined by their electrical conductivity, the transportation speed of electrolyte ions, and the nature of the active materials.[158] According to their different energy storage behaviours, supercapacitors can be classified into electrical double-layer capacitors (EDLCs) and

pseudocapacitors.[158,159] In recent years, different 3DGAs have been successfully used as electrode materials for EDLCs, owing to their high SSA, good electrical conductivity, and porous structure.[160-162] The 3D interconnected structure of graphene can be also utilized to develop binder-free electrodes. For example, Zhang et al. developed a mechanically strong and electrically conductive graphene aerogel for supercapacitors.[9] The material was fabricated by using supercritical CO_2 to dry the hydrogel precursor, which was synthesized by reducing GO with L-ascorbic acid (**Figure 12a**). The obtained graphene had a high SSA of 512 m^2 g^{-1} and an advanced 3D porous structure (**Figure 12b**). It delivered typical EDLC rectangular cyclic voltammetry (CV) curves (**Figure 12c**), with specific capacitance of 128 F g^{-1} and excellent rate performance. Sui et al. synthesized an N-doped graphene aerogel (NGA) with high porosity via a hydrothermal method (**Figure 12d** and **12e**).[163] The NGA had a high N doping concentration of 8.4 at.% and a high SSA of 814 m^2 g^{-1}. The doped N heteroatoms can help to further improve the supercapacitor performance of graphene aerogel electrode, because the doped heteroatoms are able to increase the wettability and electrical conductivity of the carbon framework. By benefiting from these advantages, NGA delivered enhanced capacitance of 223 F g^{-1} at 0.2 A g^{-1}. In addition, it had excellent capacity retention, with only 8% fading after 2000 cycles at 1 A g^{-1} (**Figure 12f**).

In spite of these advantages of 3DGAs and doped 3DGAs, their porous structure may sacrifice the volumetric energy density of the electrode. Increasing the packing density is of great importance for the practical application of 3DGA electrodes. To date, different types of 3D porous graphene electrodes with high volumetric density have been developed. For example, Xu et al. developed a 3D holey graphene framework (HGF) with a hierarchical porous structure as a high-energy-density supercapacitor electrode (**Figure 12g**).[164] The HGF had a large ion-accessible surface area and efficient transport pathways for electrons and ions. After compression, the packing density of the HGF film reached 0.71 g cm^{-3} (**Figure 12h**). Although the compressed HGF had a dense structure, its SSA was as high as

810 m^2 g^{-1}. Due to its unique structure, the HGF film exhibited a gravimetric capacitance of 298 F g^{-1} and a volumetric capacitance of 212 F cm^{-3} in organic electrolyte (**Figure 12i**). More importantly, its energy density was comparable with those of lead acid batteries.

Apart from directly acting as electrodes for supercapacitors, 3DGAs can be used in combination with active materials, including metal oxides, as well as in building hybrid structures for supercapacitors. These active materials, which normally serve as electrodes for pseudocapacitors, have high capacitances but low electrical conductivity and poor capacity retention. A 3DGA matrix can help to improve the conductivity of the active materials and provide rapid diffusion channels for the electrolyte ions. Therefore, the hybrid is able to deliver high electrochemical performance, including higher capacitance, better capacity retention, and better rate capability. For example, Wang et al. electrochemically deposited MnO_2 nanoparticles on graphene and formed a MnO_2/graphene aerogel composite (MnO_2/GA) (**Figure 13a**).[165] The composite had a high MnO_2 loading of 61 wt.% and exhibited a high capacitance of 410 F g^{-1} at 2 mVs^{-1}, which was much higher than that of pure MnO_2 (**Figure 13b**). The CV curves indicated that the energy storage mechanism of MnO_2/GA was EDLC for the graphene aerogel and pseudocapacitance for the MnO_2. The peak at ~ 0.5 V can be attributed to the surface reaction of MnO_2 and electrolyte ions (**Figure 13c**). Qu et al. synthesized a graphene/hierarchical-graphene-coupled PANI aerogel (HGC-PANI), in which PANI uniformly grew on the surfaces of the graphene nanosheets.[166] This composite possessed both localized conductivity from the graphene sandwiched between the PANI nanosheets and long-distance conductivity from the graphene framework (**Figure 13d**). As a result, the MnO_2/GA showed enhanced electrochemical performance, including higher capacitance and excellent capacity retention (90% after 3000 cycles at 100 mV s^{-1}), based on its unique structure (**Figure 13e**).

The performance of different 3DGAs and 3DGA-based composites for supercapacitor application was summarized in **Table 3**. It could be concluded that 3DGAs have delivered high supercapacitor performance as self-supported electrodes due to their porous structure and high electrical conductivity. Their volumetric energy density is far from reaching a stratification commercially viable level, however, although the construction of 3DGA electrodes with high pack density may be important for solving this problem. Developing 3DGA-based composite electrodes could improve the electrochemical performance of supercapacitors. It is worth noting that, in these 3DGA-based composite electrodes, both the 3DGAs and the active materials contribute to capacity. Structural modification of 3DGAs, by heteroatom doping, for example, could further improve the performance of supercapacitors by increasing the wettability and conductivity of the carbon framework.

6. Conclusions and prospects

We have reviewed the recent advances on 3DGAs and their composites for energy storage applications. First, the synthesis principles and strategies of 3DGAs were summarized. Second, the recent progress on 3DGAs and 3DGA-based electrodes for different energy storage devices was reviewed, including LIBs/SIBs, Li-S batteries, lithium metal batteries, other batteries, and supercapacitors. In addition, current challenges were also summarized.

3DGAs can be synthesized by CVD methods, 3D printing and GO direct growth processes, such as the gelation of GO in suspension, the template-assisted assembly method, and GO reduction-induced self-assembly of graphene. Due to their structural merits, 3DGAs can act as a binder-free electrode for energy storage systems and deliver high capacity and excellent rate capabilities. In addition, their porous nature and conductive frameworks make 3DGAs an ideal supporting matrix for various electrochemically active materials (such as metal oxides/sulfides/phosphides, Si, Sn, P, etc.), and can be used to construct composite electrodes for batteries and supercapacitors. In the composite electrodes, the 3DGA matrix could enhance the electrical conductivity of the active materials and alleviate their volume changes

during discharge/charge cycling, while the interconnected porous structure is able to provide rapid diffusion channels for electrolyte ions. Therefore, the 3DGA matrix can effectively improve the electrochemical performance of these active materials. In addition, 3DGAs can act as capsules or hosts for S and Li_2S cathodes, and improve the performance of Li-S batteries by increasing the electrical conductivity of the cathode and alleviating the shuttle effects of polysulfides. Moreover, 3DGAs can be used as scaffolds for lithium metal batteries to effectively suppress the growth of Li dendrites.

Although these are major achievements of 3DGAs in different energy storage fields, there are still some challenges that hinder their practical applications. The synthesis processes for 3DGAs at the current stage are normally complicated and costly, and developing simple and low-cost synthesis strategies could widen the application of 3DGAs. In the case of battery anode applications, the 3DGAs suffer from low ICE. Electrolyte modification and optimization of the pore structure and specific surface area of 3DGAs are of importance for overcoming this problem. Although 3DGA matrices have effectively improved the electrochemical performance of electrochemically active materials, the loading masses were relatively low. Improving the loading content of active materials could have great importance. In addition, the adhesive strength of the active materials and 3DGAs need to be further improved to increase the overall structural stability of the composite electrode. Structural modification, such as by heteroatom doping, can also increase the electrical conductivity, enrich the content of electrochemically active sites, and improve the wettability of the carbon framework. Combinations of different modification strategies, such as heteroatom doping and polar materials loading, would have synergistic effects towards improving the electrochemical performance of 3DGAs. Importantly, increasing the packing density of 3DGA electrodes would help to further increase the volumetric energy density of energy storage devices. It should be pointed out that, the 3DGAs or 3DGA-based composites are relatively fragile, and their overall mechanical properties have rarely been systematically studied. To guarantee the

strength and flexibility of 3DGAs or 3DGA-based electrodes, their viscoelastic property should be high enough to tolerate further processing in large-scale electrode fabrication and battery assembly. Furthermore, the application of 3DGAs could be extended to other battery systems, such as aqueous Zn-ion batteries or aqueous Na-ion/K-ion batteries, considering their 3D porous conductive network and high active surface area. With continuous research efforts devoted to 3DGAs design and the optimization of electrochemical techniques, more and more advanced 3DGAs or 3DGA-based electrode materials for high-performance energy storage devices are expected to be achieved.

Acknowledgements

Zhijie Wang and Hong Gao contributed equally to this paper. Financial support provided by the Australian Research Council (ARC) (FT150100109 and DP170102406) is gratefully acknowledged. Zhijie Wang acknowledges the China Scholarship Council (CSC) for his scholarship support (Grant No. 201706340049). The authors would like to thank Dr. Tania Silver for critical reading of the manuscript and valuable remarks.

Received: ((will be filled in by the editorial staff))
Revised: ((will be filled in by the editorial staff))
Published online: ((will be filled in by the editorial staff))

References

[1] K. S. Novoselov, A. K. Geim, S. V. Morozov, D. Jiang, Y. Zhang, S. V. Dubonos, I. V. Grigorieva, A. A. Firsov, *Science* **2004,** *306*, 666-669.

[2] V. Chabot, D. Higgins, A. Yu, X. Xiao, Z. Chen, J. Zhang, *Energy Environ. Sci.* **2014,** *7*, 1564-1596.

[3] P. Song, X. Zhang, M. Sun, X. Cui, Y. Lin, *Nanoscale* **2012,** *4*, 1800-1804.

[4] X. Wu, J. Zhou, W. Xing, G. Wang, H. Cui, S. Zhuo, Q. Xue, Z. Yan, S. Z. Qiao, *J. Mater. Chem.* **2012,** *22*, 23186-23193.

[5] J. Mao, J. Iocozzia, J. Huang, K. Meng, Y. Lai, Z. Lin, *Energy Environ. Sci.* **2018**, *11*, 772-799.

[6] Y. Ma, Y. Chen, *Natl. Sci. Rev.* **2015**, *2*, 40-53.

[7] W. L. Song, X. T. Guan, L. Z. Fan, W. Q. Cao, C. Y. Wang, M. S. Cao, *Carbon* **2015**, *93*, 151-160.

[8] S. Ye, J. Feng, P. Wu, *ACS Appl. Mater. Interfaces* **2013**, *5*, 7122-7129.

[9] X. Zhang, Z. Sui, B. Xu, S. Yue, Y. Luo, W. Zhan, B. Liu, *J. Mater. Chem.* **2011,** *21*, 6494-6497.

[10] K. S. Novoselov, V. I. Fal′ko, L. Colombo, P. R. Gellert, M. G. Schwab, K. Kim, *Nature* **2012**, *490*, 192-200.

[11] L. Ren, K. N. Hui, K. S. Hui, Y. Liu, X. Qi, J. Zhong, Y. Du, J. Yang, *Sci. Rep.* **2015**, *5*, 14229.

[12] J. Wang, F. Fang, T. Yuan, J. Yang, L. Chen, C. Yao, S. Zheng, D. Sun, *ACS Appl. Mater. Interfaces* **2017**, *9*, 3544-3553.

[13] F. Jin, Y. Wang, *J. Mater. Chem. A* **2015**, *3*, 14741-14749.

[14] Z. Y. Sui, P. Y. Zhang, M. Y. Xu, Y. W. Liu, Z. X. Wei, B. H. Han, *ACS Appl. Mater. Interfaces* **2017**, *9*, 43171-43178.

[15] Y. Zhao, J. Liu, Y. Hu, H. Cheng, C. Hu, C. Jiang, L. Jiang, A. Cao, L. Qu, *Adv. Mater.* **2012**, *25*, 591-595.

[16] J. van den Brink, *Nat. Mater.* **2010,** *9*, 291-292.

[17] M. H. Rümmeli, C. G. Rocha, F. Ortmann, I. Ibrahim, H. Sevincli, F. Börrnert, J. Kunstmann, A. Bachmatiuk, M. Pötschke, M. Shiraishi, M. Meyyappan, B. Büchner, S. Roche, G. Cuniberti, *Adv. Mater.* **2011**, *23*, 4471-4490.

[18] S. Park, R. S. Ruoff, *Nat. Nanotech.* **2009**, *4*, 217-224.

[19] J. Kim, L. J. Cote, F. Kim, W. Yuan, K. R. Shull, J. Huang, *J Am. Chem. Soc.* **2010**, *132*, 8180-8186.

[20] C. Zhang, L. Ren, X. Wang, T. Liu, *J. Phys. Chem. C* **2010**, *114*, 11435-11440.

[21] Y. Xu, G. Shi, *J. Mater. Chem.* **2011**, *21*, 3311-3323.

[22] Y. Wu, B. Yang, B. Zong, H. Sun, Z. Shen, Y. Feng, *J. Mater. Chem.* **2004**, *14*, 469-477.

[23] Z. Xu, Y. Zhang, P. Li, C. Gao, *ACS Nano* **2012**, *6*, 7103-7113.

[24] X. Fan, X. Chen, L. Dai, *Curr. Opin. Colloid Interface Sci.* **2015**, *20*, 429-438.

[25] U. Patil, S. C. Lee, S. Kulkarni, J. S. Sohn, M. S. Nam, S. Han, S. C. Jun, *Nanoscale* **2015**, *7*, 6999-7021.

[26] Z. Chen, C. Xu, C. Ma, W. Ren, H. M. Cheng, *Adv. Mater.* **2013**, *25*, 1296-1300.

[27] Z. Chen, W. Ren, L. Gao, B. Liu, S. Pei, H. M. Cheng, *Nat. Mater.* **2011**, *10*, 424-428.

[28] X. Cao, Y. Shi, W. Shi, G. Lu, X. Huang, Q. Yan, Q. Zhang, H. Zhang, *Small*, **2011**, *7*, 3163-3168.

[29] L. Cipelletti, L. Ramos, *Curr. Opin. Colloid Interface Sci.* **2002**, *7*, 228-234.

[30] H. Bai, C. Li, X. Wang, G. Shi, *Chem. Commun.* **2010**, *46*, 2376-2378.

[31] B. Konkena, S. Vasudevan, *J. Phys. Chem. C* **2014**, *118*, 21706-21713.

[32] S. M. Jung, H. Y. Jung, M. S. Dresselhaus, Y. J. Jung, J. Kong, *Sci. Rep.* **2012**, *2*, 849.

[33] B. Adhikari, A. Biswas, A. Banerjee, *ACS Appl. Mater. Interfaces* **2012**, *4*, 5472-5482.

[34] H. Hu, Z. Zhao, W. Wan, Y. Gogotsi, J. Qiu, *Adv. Mater.* **2013**, *25*, 2219-2223.

[35] X. Ma, Y. Li, W. Wang, Q. Ji, Y. Xia, *Eur. Polym. J.* **2013**, *49*, 389-396.

[36] H. Bai, C. Li, X. Wang, G. Shi, *J. Phys. Chem. C* **2011**, *115*, 5545-5551.

[37] C. K. Chua, M. Pumera, *Chem. Soc. Rev.* **2014**, *43*, 291-312.

[38] W. Lv, Y. Tao, W. Ni, Z. Zhou, F. Y. Su, X. C. Chen, F.-M. Jin, Q. H. Yang, *J. Mater. Chem.* **2011**, *21*, 12352-12357.

[39] Z. Tang, S. Shen, J. Zhuang, X. Wang, *Angew. Chem. Int. Ed.* **2010**, *122*, 4707-4711.

[40] Y. Chen, L. Chen, H. Bai, L. Li, *J. Mater. Chem. A* **2013**, *1*, 1992-2001.

[41] J.-J. Shao, W. Lv, Q. H. Yang, *Adv. Mater.* **2014**, *26*, 5586-5612.

[42] J. Chen, K. Sheng, P. Luo, C. Li, G. Shi, *Adv. Mater.* **2012**, *24*, 4569-4573.

[43] T. Zhai, X. Lu, H. Wang, G. Wang, T. Mathis, T. Liu, C. Li, Y. Tong, Y. Li, *Nano Lett.* **2015**, *15*, 3189-3194.

[44] L. Qiu, Z. Liu, L.Y. Chang, Y. Wu, D. Li, *Nat. Commun.* **2012**, *3*, 1241.

[45] D. Parviz, S. D. Metzler, S. Das, F. Irin, M. J. Green, *Small* **2015**, *11*, 2661-2668.

[46] A. Zhang, H. Bai, L. Li, *Chem. Rev.* **2015**, *115*, 9801-9868.

[47] H. Sun, Z. Xu, C. Gao, *Adv. Mater.* **2013**, *25*, 2554-2560.

[48] Z. Yu, M. McInnis, J. Calderon, S. Seal, L. Zhai, J. Thomas, *Nano Energy* **2015**, *11*, 611-620.

[49] H. Tang, P. Gao, Z. Bao, B. Zhou, J. Shen, Y. Mei, G. Wu, *Nano Res.* **2014**, *8*, 1710-1717.

[50] Y. Xu, K. Sheng, C. Li, G. Shi, *ACS Nano* **2010**, *4*, 4324-4330.

[51] W. Lv, C. Zhang, Z. Li, Q. H. Yang, *J. Phys. Chem. Lett.* **2015**, *6*, 658-668.

[52] W. Chen, L. Yan, *Nanoscale* **2011**, *3*, 3132-3137.

[53] M. A. Worsley, S. O. Kucheyev, H. E. Mason, M. D. Merrill, B. P. Mayer, J. Lewicki, C. A. Valdez, M. E. Suss, M. Stadermann, P. J. Pauzauskie, J. H. Satcher, J. Biener, T. F. Baumann, *Chem. Commun.* **2012**, *48*, 8428-8430.

[54] A. P. Goldstein, W. Mickelson, A. Machness, G. Lee, M. A. Worsley, L. Woo, A. Zettl, *J. Phys. Chem. C* **2014**, *118*, 28855-28860.

[55] C. Cheng, D. Li, *Adv. Mater.* **2012**, *25*, 13-30.

[56] X. Xie, Y. Zhou, H. Bi, K. Yin, S. Wan, L. Sun, *Sci. Rep.* **2013**, *3*, 2117.

[57] Z. Han, Z. Tang, S. Shen, B. Zhao, G. Zheng, J. Yang, *Sci. Rep.* **2014**, *4*, 5025.

[58] Yao, J. Chen, L. Huang, Q. Zhou, G. Shi, *Adv. Mater.* **2015**, *28*, 1623-1629.

[59] Q. Zhang, F. Zhang, S. P. Medarametla, H. Li, C. Zhou, D. Lin, *Small*, **2016**, *13*, 1702-1708.

[60] E. García-Tuñon, S. Barg, J. Franco, R. Bell, S. Eslava, E. D'Elia, R. C. Maher, F. Guitian, E. Saiz, *Adv. Mater.* **2015**, *27*, 1688-1693.

[61] K. Fu, Y. Yao, J. Dai, L. Hu, *Adv. Mater.* **2017**, *29*, 1603486.

[62] D. Lin, S. Jin, F. Zhang, C. Wang, Y. Wang, C. Zhou, G. Cheng, *Nanotechnology*, **2015**, *26*, 434003.

[63] X. Wei, D. Li, W. Jiang, Z. Gu, X. Wang, Z. Zhang, Z. Sun, *Sci. Rep.* **2015**, *5*, 11181.

[64] C. Zhu, T. Y. Han, E. B. Duoss, A. E. Golobic, J. D. Kuntz, C. M. Spadaccini, M. A. Worsley, *Nat. Commun.* **2015**, *6*, 6962.

[65] C. Zhu, T. Liu, F. Qian, T. Y. Han, E. B. Duoss, J. D. Kuntz, C. M. Spadaccini, M. A. Worsley, Y. Li, *Nano Lett.* **2016**, *16*, 3448-3456.

[66] J. Biener, M. Stadermann, M. Suss, M. A. Worsley, M. M. Biener, K. A. Rose, T. F. Baumann, *Energy Environ. Sci.* **2011**, *4*, 656-667.

[67] S. Han, D. Wu, S. Li, F. Zhang, X. Feng, *Adv. Mater.* **2013**, *26*, 849-864.

[68] Z. S. Wu, Y. Sun, Y. Z. Tan, S. Yang, X. Feng, K. Müllen, *J. Am. Chem. Soc.* **2012**, *134*, 19532-19535.

[69] Y. Wang, Z. Wang, X. Yu, B. Li, F. Kang, Y. B. He, *J. Mater. Res.* **2018**, *33*, 1058-1073.

[70] Z. Wang, X. Yu, W. He, Y. V. Kaneti, D. Han, Q. Sun, Y. B. He, B. Xiang, *ACS Appl. Mater. Interfaces* **2016**, *8*, 33399-33404.

[71] Z. Wang, Y. Wang, W. Wang, X. Yu, W. Lv, B. Xiang, Y.-B. He, *Front. Chem.* **2018**, *6*, 97.

[72] X. Yu, C. Zhan, R. Lv, Y. Bai, Y. Lin, Z. H. Huang, W. Shen, X. Qiu, F. Kang, *Nano Energy* **2015**, *15*, 43-53.

[73] G. Wang, X. Shen, J. Yao, J. Park, *Carbon* **2009**, *47*, 2049-2053.

[74] Y. S. Yun, Y. U. Park, S. J. Chang, B. H. Kim, J. Choi, J. Wang, D. Zhang, P. V. Braun, H. J. Jin, K. Kang, *Carbon* **2016**, *99*, 658-664.

[75] Z. Zuo, T. Y. Kim, I. Kholmanov, H. Li, H. Chou, Y. Li, *Small* **2015**, *11*, 4922-4930.

[76] J. Zhang, C. Li, Z. Peng, Y. Liu, J. Zhang, Z. Liu, D. Li, *Sci. Rep.* **2017**, *7*, 4886.

[77] J. Zhang, W. Lv, Y. Tao, Y.-B. He, D.-W. Wang, C.-H. You, B. Li, F. Kang, Q. H. Yang, *Energy Storage Mater.* **2015**, *1*, 112-118.

[78] Y. Xu, Z. Lin, X. Zhong, B. Papandrea, Y. Huang, X. Duan, *Angew. Chem. Int. Ed.* **2015**, *127*, 5435-5440.

[79] J. Y. Hong, J. J. Wie, Y. Xu, H. S. Park, *Phys. Chem. Chem. Phys.* **2015**, *17*, 30946-30962.

[80] D. Li, D. Shi, Z. Liu, H. Liu, Z. Guo, *J. Nanopart. Res.* **2013**, *15*, 1674.

[81] M. Jiang, T. Zhou, W. Liu, C. Feng, J. Liu, Z. Guo, *RSC Adv.* **2017**, *7*, 17769-17772.

[82] D. Bai, F. Wang, J. Lv, F. Zhang, S. Xu, *ACS Appl. Mater. Interfaces* **2016**, *8*, 32853-32861.

[83] M. A. Garakani, S. Abouali, B. Zhang, C. A. Takagi, Z. L. Xu, J.Q. Huang, J. Huang, J. K. Kim, *ACS Appl. Mater. Interfaces* **2014**, *6*, 18971-18980.

[84] J. Meng, Y. Cao, Y. Suo, Y. Liu, J. Zhang, X. Zheng, *Electrochim. Acta* **2015**, *176*, 1001-1009.

[85] J. K. Meng, L. Fu, Y. S. Liu, G.-P. Zheng, X. C. Zheng, X. X. Guan, J. M. Zhang, *Electrochim. Acta* **2017**, *224*, 40-48.

[86] B. Qiu, Y. Deng, M. Du, M. Xing, J. Zhang, *Sci. Rep.* **2016**, *6*, 29099.

[87] L. Xiao, D. Wu, S. Han, Y. Huang, S. Li, M. He, F. Zhang, X. Feng, *ACS Appl. Mater. Interfaces* **2013**, *5*, 3764-3769.

[88] X. Yao, G. Guo, X. Ma, Y. Zhao, C. Y. Ang, Z. Luo, K. T. Nguyen, P. Z. Li, Q. Yan, Y. Zhao, *ACS Appl. Mater. Interfaces* **2015**, *7*, 26085-26093.

[89] T. Jiang, F. Bu, X. Feng, I. Shakir, G. Hao, Y. Xu, *ACS Nano* **2017**, *11*, 5140-5147.

[90] W. S. V. Lee, E. Peng, T. A. J. Loh, X. Huang, J. M. Xue, *Nanoscale* **2016**, *8*, 8042-8047.

[91] X. T. Gao, Y. T. Liu, X. D. Zhu, D. J. Yan, C. Wang, Y. J. Feng, K. N. Sun, *Carbon* **2018**, *140*, 218-226.

[92] Y. Zhou, Q. Liu, D. Liu, H. Xie, G. Wu, W. Huang, Y. Tian, Q. He, A. Khalil, Y. A. Haleem, T. Xiang, W. Chu, C. Zou, L. Song, *Electrochim. Acta* **2015**, *174*, 8-14.

[93] W. Wei, S. Yang, H. Zhou, I. Lieberwirth, X. Feng, K. Müllen, *Adv. Mater.* **2013**, *25*, 2909-2914.

[94] P. Chang, X. Liu, Q. Zhao, Y. Huang, Y. Huang, X. Hu, *ACS Appl. Mater. Interfaces* **2017**, *9*, 31879-31886.

[95] Z. Yang, K. Qian, J. Lv, W. Yan, J. Liu, J. Ai, Y. Zhang, T. Guo, X. Zhou, S. Xu, Z. Guo, *Sci. Rep.* **2016**, *6*, 27957.

[96] D. He, L. Li, F. Bai, C. Zha, L. Shen, H. H. Kung, N. Bao, *Chem. Eur. J.* **2016**, *22*, 4454-4459.

[97] C. Tan, J. Cao, A. M. Khattak, F. Cai, B. Jiang, G. Yang, S. Hu, *J. Power Sources* **2014**, *270*, 28-33.

[98] D. Xie, W. J. Tang, X. H. Xia, D. H. Wang, D. Zhou, F. Shi, X. L. Wang, C. D. Gu, J. P. Tu, *J. Power Sources* **2015**, *296*, 392-399.

[99] Z. Li, J. Ding, D. Mitlin, *Accounts Chem. Res.* **2015**, *48*, 1657-1665.

[100] J. Qian, X. Wu, Y. Cao, X. Ai, H. Yang, *Angew. Chem. Int. Ed.* **2013**, *125*, 4731-4734.

[101] B. Luo, T. Qiu, D. Ye, L. Wang, L. Zhi, *Nano Energy* **2016**, *22*, 232-240.

[102] J. Sun, H. W. Lee, M. Pasta, H. Yuan, G. Zheng, Y. Sun, Y. Li, Y. Cui, *Nat. Nanotech.* **2015**, *10*, 980-985.

[103] H. Gao, T. Zhou, Y. Zheng, Y. Liu, J. Chen, H. Liu, Z. Guo, *Adv. Energy Mater.* **2016**, *6*, 1601037.

[104] F. Pan, W. Zhang, J. Ma, N. Yao, L. Xu, Y. S. He, X. Yang, Z. F. Ma, *Electrochim. Acta* **2016**, *196*, 572-578.

[105] N. Li, S. Liao, Y. Sun, H. W. Song, C. X. Wang, *J. Mater. Chem. A* **2015**, *3*, 5820-5828.

[106] H. Liu, M. Jia, Q. Zhu, B. Cao, R. Chen, Y. Wang, F. Wu, B. Xu, *ACS Appl. Mater. Interfaces* **2016**, *8*, 26878-26885.

[107] Y. Liu, Z. Cheng, H. Sun, H. Arandiyan, J. Li, M. Ahmad, *J. Power Sources* **2015**, *273*, 878-884.

[108] Y. Zheng, T. Zhou, C. Zhang, J. Mao, H. Liu, Z. Guo, *Angew. Chem. Int. Ed.* **2016**, *128*, 3469-3474.

[109] Z. Li, J. Ding, H. Wang, K. Cui, T. Stephenson, D. Karpuzov, D. Mitlin, *Nano Energy* **2015**, *15*, 369-378.

[110] X. Hu, J. Chen, G. Zeng, J. Jia, P. Cai, G. Chai, Z. Wen, *J. Mater. Chem. A* **2017**, *5*, 23460-23470.

[111] Y. Lu, N. Zhang, S. Jiang, Y. Zhang, M. Zhou, Z. Tao, L. A. Archer, J. Chen, *Nano Lett.* **2017**, *17*, 3668-3674.

[112] J. Xiang, D. Dong, F. Wen, J. Zhao, X. Zhang, L. Wang, Z. Liu, *J. Alloy Compd.* **2016**, *660*, 11-16.

[113] X. Hu, Y. Li, G. Zeng, J. Jia, H. Zhan, Z. Wen, *ACS Nano* **2018**, *12*, 1592-1602.

[114] Y. Wang, D. Kong, W. Shi, B. Liu, G. J. Sim, Q. Ge, H. Y. Yang, *Adv. Energy Mater.* **2016**, *6*, 1601057.

[115] Y. Zhang, L. Fan, P. Wang, Y. Yin, X. Zhang, N. Zhang, K. Sun, *Nanoscale* **2017**, *9*, 17694-17698.

[116] M. Armand, J. M. Tarascon, *Nature* **2008**, *451*, 652-657.

[117] P. G. Bruce, S. A. Freunberger, L. J. Hardwick, J. M. Tarascon, *Nat. Mater.* **2011**, *11*, 19-29.

[118] L. Zhang, Y. Wang, B. Peng, W. Yu, H. Wang, T. Wang, B. Deng, L. Chai, K. Zhang, J. Wang, *Green Chem.* **2014**, *16*, 3926-3934.

[119] H. Wang, W. Zhang, J. Xu, Z. Guo, *Adv. Funct. Mater.* **2018**, 1707520.

[120] X. Ji, K. T. Lee, L. F. Nazar, *Nat. Mater.* **2009**, *8*, 500-506.

[121] Y. You, W. Zeng, Y. X. Yin, J. Zhang, C. P. Yang, Y. Zhu, Y. G. Guo, *J. Mater. Chem. A* **2015**, *3*, 4799-4802.

[122] C. Nan, Z. Lin, H. Liao, M. K. Song, Y. Li, E. J. Cairns, *J. Am. Chem. Soc.* **2014**, *136*, 4659-4663.

[123] G. Zhou, E, Park, G. S. Hwang, A. Manthiram, *Nat. Commun.* **2015**, *6*, 7760.

[124] F. Nitze, M. Agostini, F. Lundin, A. E. C. Palmqvist, A. Matic, *Sci. Rep.* **2016**, *6*,

39615.

[125] C. Tang, Q. Zhang, M. Q. Zhao, J. Q. Huang, X. B. Cheng, G. L. Tian, H. J. Peng, F. Wei, *Adv. Mater.* **2014**, *26*, 6100-6105.

[126] Y. J. Choi, B. S. Jung, D. J. Lee, J. H. Jeong, K. W. Kim, H. J. Ahn, K. K. Cho, H. B. Gu, *Phys. Scr.* **2007**, *2007*, 62.

[127] S. Evers, T. Yim, L. F. Nazar, *J. Phys. Chem. C* **2012**, *116*, 19653-19658.

[128] X. Ji, S. Evers, R. Black, L. F. Nazar, *Nat. Commun.* **2011**, *2*, 325.

[129] F. Sun, J. Wang, D. Long, W. Qiao, L. Ling, C. Lv, R. Cai, *J. Mater. Chem. A* **2013**, *1*, 13283-13289.

[130] Y. Zhang, Y. Zhao, A. Yermukhambetova, Z. Bakenov, P. Chen, *J. Mater. Chem. A* **2013**, *1*, 295-301.

[131] J. He, Y. Chen, W. Lv, K. Wen, C. Xu, W. Zhang, W. Qin, W. He, *ACS Energy Lett.* **2016**, *1*, 820-826.

[132] M. Liu, Z. Yang, H. Sun, C. Lai, X. Zhao, H. Peng, T. Liu, *Nano Res.* **2016**, *9*, 3735-3746.

[133] Y. Fu, Y. S. Su, A. Manthiram, *J. Electrochem. Soc.* **2012**, *159*, A1420-A1424.

[134] J. Song, M. L. Gordin, T. Xu, S. Chen, Z. Yu, H. Sohn, J. Lu, Y. Ren, Y. Duan, D. Wang, *Angew. Chem. Int. Ed.* **2015**, *127*, 4399-4403.

[135] F. Wu, J. Chen, R. Chen, S. Wu, L. Li, S. Chen, T. Zhao, *J. Phys. Chem. C* **2011**, *115*, 6057-6063.

[136] W. Zhou, Y. Yu, H. Chen, F. J. DiSalvo, H. D. Abruña, *J. Am. Chem. Soc.* **2013**, *135*, 16736-16743.

[137] K. Zhang, K. Xie, K. Yuan, W. Lu, S. Hu, W. Wei, M. Bai, C. Shen, *J. Mater. Chem. A* **2017**, *5*, 7309-7315.

[138] J. Q. Huang, Z. Wang, Z. L. Xu, W. G. Chong, X. Qin, X. Wang, J. K. Kim, *ACS Appl. Mater. Interfaces* **2016**, *8*, 28663-28670.

[139] M. Yu, A. Wang, F. Tian, H. Song, Y. Wang, C. Li, J. D. Hong, G. Shi, *Nanoscale* **2015**, *7*, 5292-5298.

[140] Z. Jiao, L. Chen, J. Si, C. Xu, Y. Jiang, Y. Zhu, Y. Yang, B. Zhao, *J. Power Sources* **2017**, *353*, 167-175.

[141] J. Song, T. Xu, M. L. Gordin, P. Zhu, D. Lv, Y. B. Jiang, Y. Chen, Y. Duan, D. Wang, *Adv. Funct. Mater.* **2013**, *24*, 1243-1250.

[142] C. Wang, K. Su, W. Wan, H. Guo, H. Zhou, J. Chen, X. Zhang, Y. Huang, *J. Mater. Chem. A* **2014**, *2*, 5018-5023.

[143] Y. Xie, Z. Meng, T. Cai, W. Q. Han, *ACS Appl. Mater. Inter.* **2015**, *7*, 25202-25210.

[144] G. Zhou, E. Paek, G. S. Hwang, A. Manthiram, *Adv. Energy Mater.* **2015**, *6*, 1501355.

[145] W. Xu, J. Wang, F. Ding, X. Chen, E. Nasybulin, Y. Zhang, J. G. Zhang, *Energy Environ. Sci.* **2014**, *7*, 513-537.

[146] C. Monroe, J. Newman, *J. Electrochem. Soc.* **2003**, *150*, A1377-A1384.

[147] D. Lin, Y. Liu, Y. Cui, *Nat. Nanotech.* **2017**, *12*, 194-206.

[148] Y. Wang, Z. Wang, D. Lei, W. Lv, Q. Zhao, B. Ni, Y. Liu, B. Li, F. Kang, Y. B. He, *ACS Appl. Mater. Interfaces* **2018**, *10*, 20244-20249.

[149] C. P. Yang, Y. X. Yin, S. F. Zhang, N. W. Li, Y. G. Guo, *Nat. Commun.* **2015**, *6*, 805.

[150] Q. Yun, Y. B. He, W. Lv, Y. Zhao, B. Li, F. Kang, Q. H. Yang, *Adv. Mater.* **2016**, *28*, 6932-6939.

[151] S. Jin, Z. Sun, Y. Guo, Z. Qi, C. Guo, X. Kong, Y. Zhu, H. Ji, *Adv. Mater.* **2017**, *29*, 1700783.

[152] D. Lin, Y. Liu, Z. Liang, H. W. Lee, J. Sun, H. Wang, K. Yan, J. Xie, Y. Cui, *Nat. Nanotech.* **2016**, *11*, 626-632.

[153] J. Zhao, G. Zhou, K. Yan, J. Xie, Y. Li, L. Liao, Y. Jin, K. Liu, P. C. Hsu, J. Wang, H. M. Cheng, Y. Cui, *Nat. Nanotech.* **2017**, *12*, 993-999.

[154] J. He, Y. Chen, W. Lv, K. Wen, P. Li, Z. Wang, W. Zhang, W. Qin, W. He, *ACS Energy*

Lett. **2016**, *1*, 16-20.

[155] J. Jiang, P. He, S. Tong, M. Zheng, Z. Lin, X. Zhang, Y. Shi, H. Zhou, *NPG Asia Materials* **2016**, *8*, e239.

[156] S. Hu, T. Han, C. Lin, W. Xiang, Y. Zhao, P. Gao, F. Du, X. Li, Y. Sun, *Adv. Funct. Mater.* **2017**, *27*, 1700041.

[157] X. Li, L. Zhi, *Chem. Soc. Rev.* **2018**, *47*, 3189-3216.

[158] G. Wang, L. Zhang, J. Zhang, *Chem. Soc. Rev.* **2012**, *41*, 797-828.

[159] L. L. Zhang, R. Zhou, X. S. Zhao, *J. Mater. Chem.* **2010**, *20*, 5983-5992.

[160] H. Kim, M.Y. Cho, M.H. Kim, K.Y. Park, H. Gwon, Y. Lee, K. C. Roh, K. Kang, *Adv. Energy Mater.* **2013**, *3*, 1500-1506.

[161] Y. Song, T. Liu, F. Qian, C. Zhu, B. Yao, E. Duoss, C. Spadaccini, M. Worsley, Y. Li, *J. Colloid Interf. Sci* **2018**, *509*, 529-545

[162] X. L. Wu, A. W. Xu, *J. Mater. Chem. A* **2014**, *2*, 4852-4864.

[163] Z. Y. Sui, Y. N. Meng, P. W. Xiao, Z. Q. Zhao, Z. X. Wei, B. H. Han, *ACS Appl. Mater. Interfaces* **2015**, *7*, 1431-1438.

[164] Y. Xu, Z. Lin, X. Zhong, X. Huang, N. O. Weiss, Y. Huang, X. Duan, *Nat. Commun.* **2014**, *5*, 4554.

[165] C. C. Wang, H. C. Chen, S. Y. Lu, *Chem. Eur. J.* **2013**, *20*, 517-523.

[166] Y. Qu, C. Lu, Y. Su, D. Cui, Y. He, C. Zhang, M. Cai, F. Zhang, X. Feng, X. Zhuang, *Carbon* **2018**, *127*, 77-84.

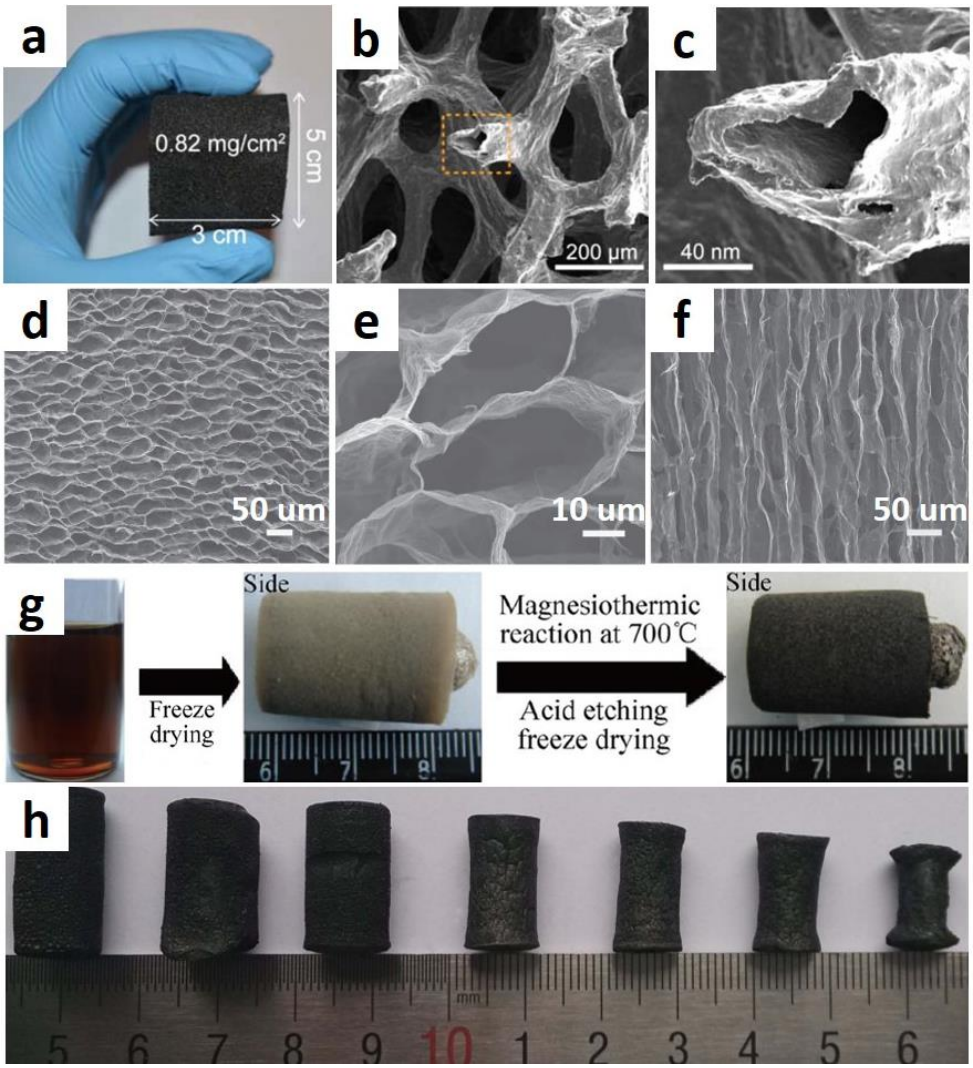

Figure 1. (a) Digital micrograph of a 3 cm×5 cm 3DGH substrate with a mass density of 0.82 mg/cm^2; (b) Low-magnification and (c) high-magnification scanning electron microscope (SEM) image of a 3DGH structure;[43] Reproduced with permission, Copyright 2015, American Chemical Society. (d-f) SEM images of graphene monolith at different magnifications: (d, e) typical top-view and (f) side-view;[44] Reproduced with permission, Copyright 2012, Springer Nature. (g) Synthesis process for 3DGAs via magnesiothermic reaction;[49] Reproduced with permission, Copyright 2015, Springer Nature. (h) Photographs of graphene aerogel prepared in different ammonium concentrations with the same mass and different volumes: a-GA-10%, a-GA-12%, a-GA-14%, a-GA-16%, a-GA-18%, a-GA-20%, and a-GA-22% (from left to right).[57] Reproduced with permission, Copyright 2014, Springer Nature.

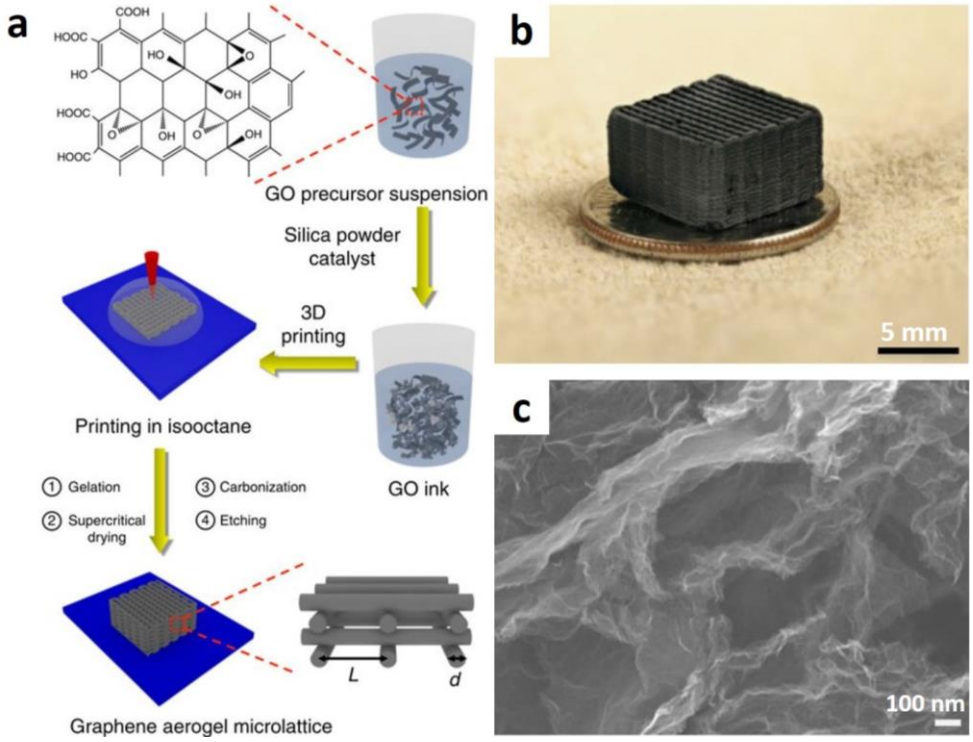

Figure 2. (a) Synthsis process for a 3D-printed graphene aerogel microlattice; (b) Digital photograph and (c) SEM image of the 3D-printed graphene aerogel microlattice.[64] Reproduced with permission, Copyright 2015, Springer Nature.

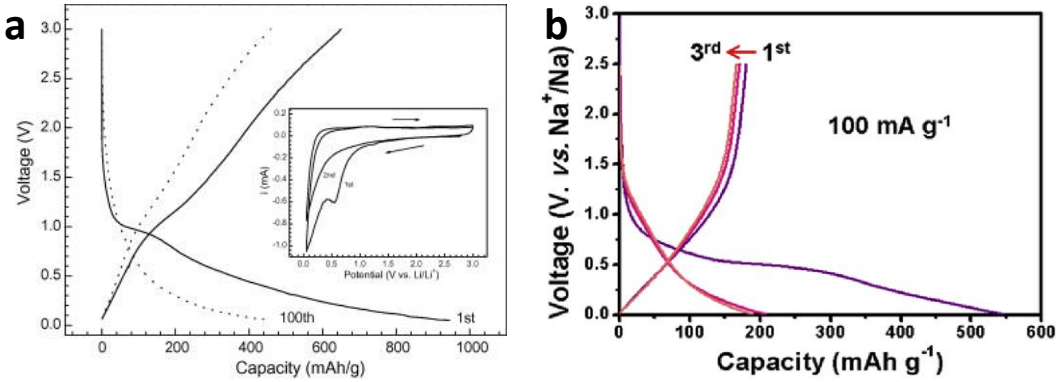

Figure 3. (a) Discharge-charge curves of the first two cycles and corresponding CV curves (inset) of graphene as anode for LIBs;[73] Reproduced with permission, Copyright 2009, Elsevier. (b) Discharge-charge curves of the first three cycle of graphene as anode for SIBs.[74] Reproduced with permission, Copyright 2016, Elsevier.

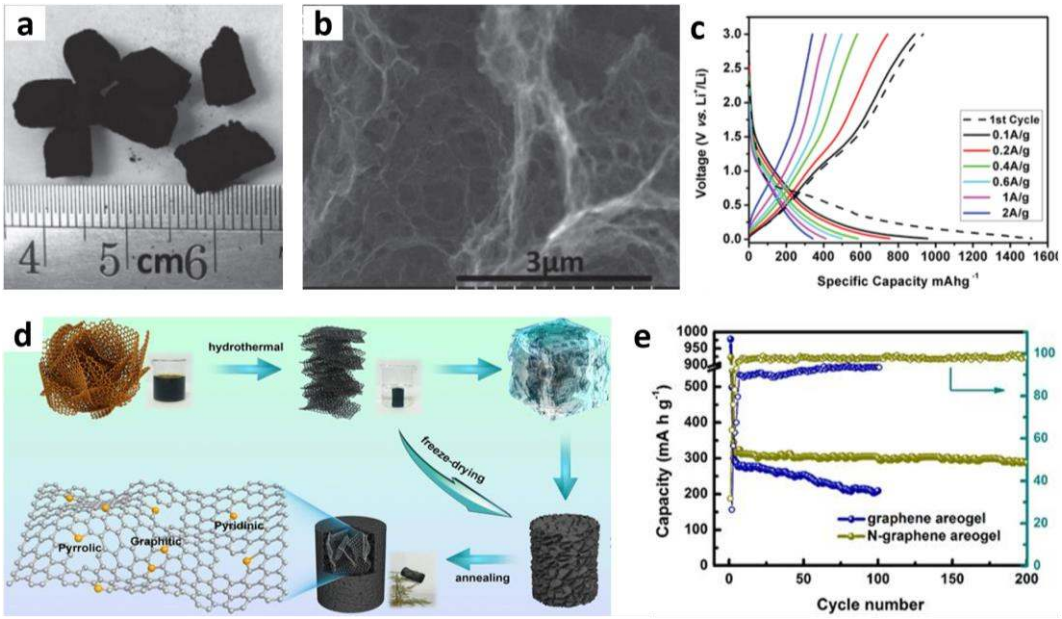

Figure 4. (a) Photograph and (b) SEM image of the 3D graphene foam, (c) Discharge-charge curves at different current densities of 3D graphene as anode for LIBs;[75] Reproduced with permission, Copyright 2015, John Wiley and Sons. (d) Schematic illustration of the synthesis approach and the application of 3D rGO aerogel, (e) Cycling performance and corresponding Coulombic efficiency of the 3D rGO aerogel.[76] Reproduced with permission, Copyright 2017, Springer Nature.

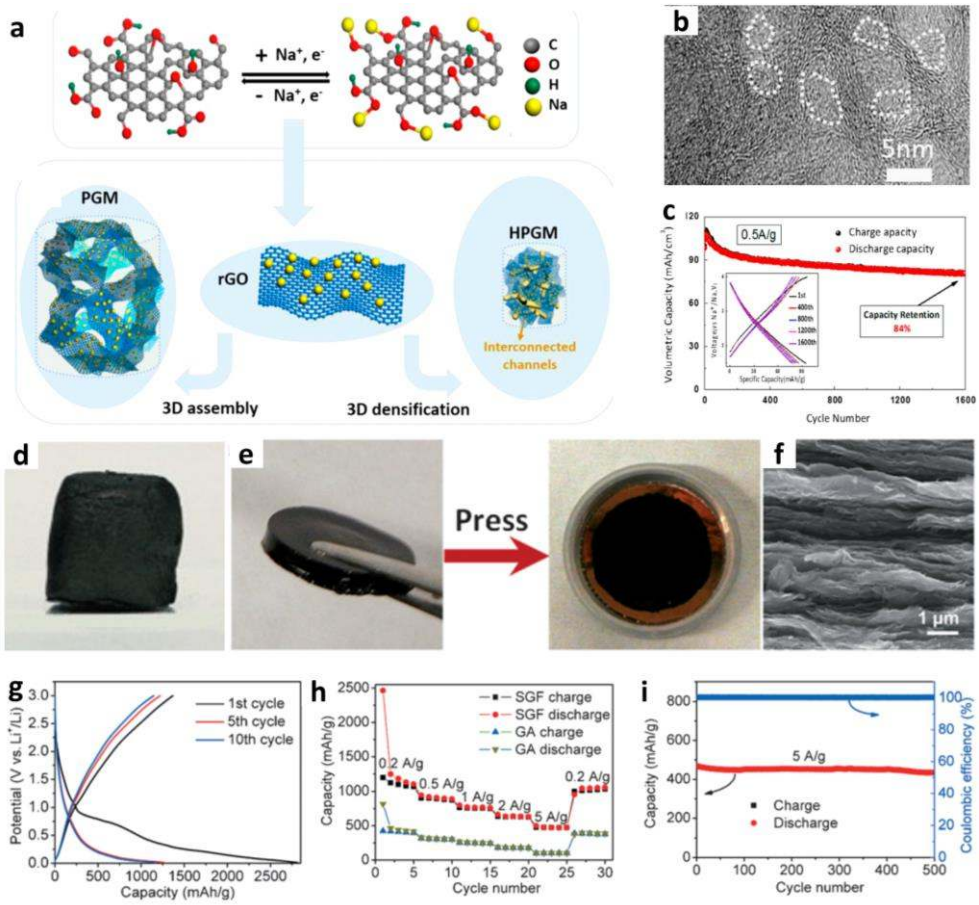

Figure 5. (a) Schematic illustration of HPGM as anode for SIBs, (b) Transmission electron microscope (TEM) image of HPGM, (c) Cycling performance and corresponding discharge-charge curves of HPGM;[77] Reproduced with permission, Copyright 2015, Elsevier. (d) Photograph of the graphene aerogel prepared from graphene hydrogel, (e) Photograph of the pressed SGF electrode, (f) SEM image of the pressed SGF electrode, (g) Discharge-charge curves, (h) rate capabilities, and (i) long cycling test at high discharge rate of the SGF.[78] Reproduced with permission, Copyright 2015, John Wiley and Sons.

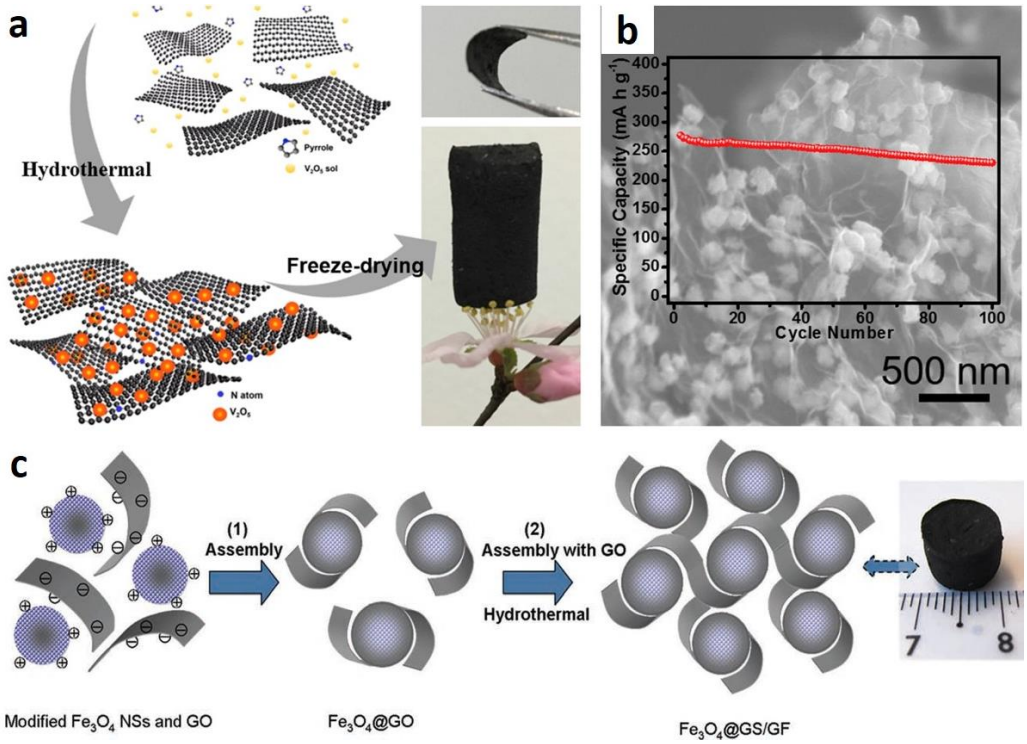

Figure 6. (a) Schematic illustration of the synthesis of V_2O_5@graphene aerogel, and corresponding photographs, (b) SEM image of V_2O_5@graphene aerogel and its cycling performance (inset);[91] Reproduced with permission, Copyright 2018, Elsevier. (c) Fabrication process and photograph of Fe_3O_4@GS/GF.[93] Reproduced with permission, Copyright 2018, Elsevier.

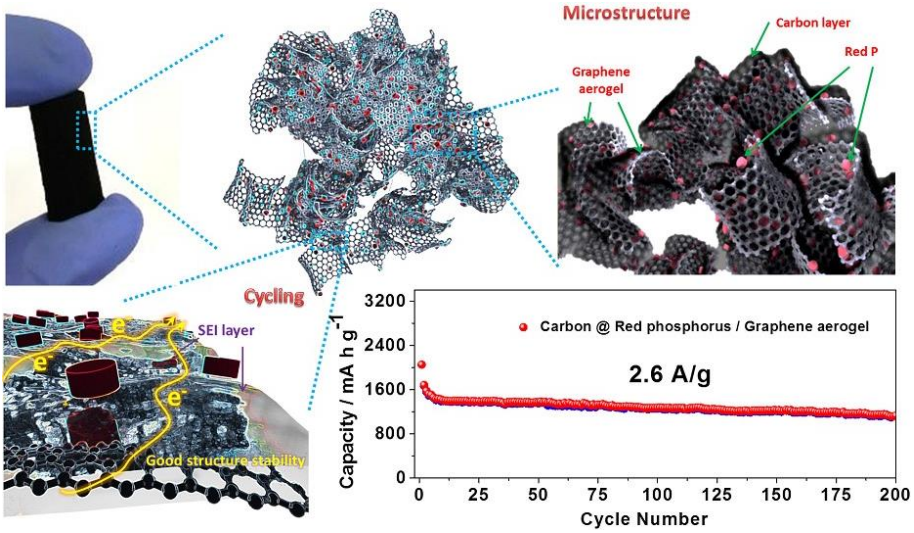

Figure 7. Photograph of the C@P/GA, and schematic illustration of its structural advantages, as well as its Na^+ storage performance.[103] Reproduced with permission, Copyright 2016, John Wiley and Sons.

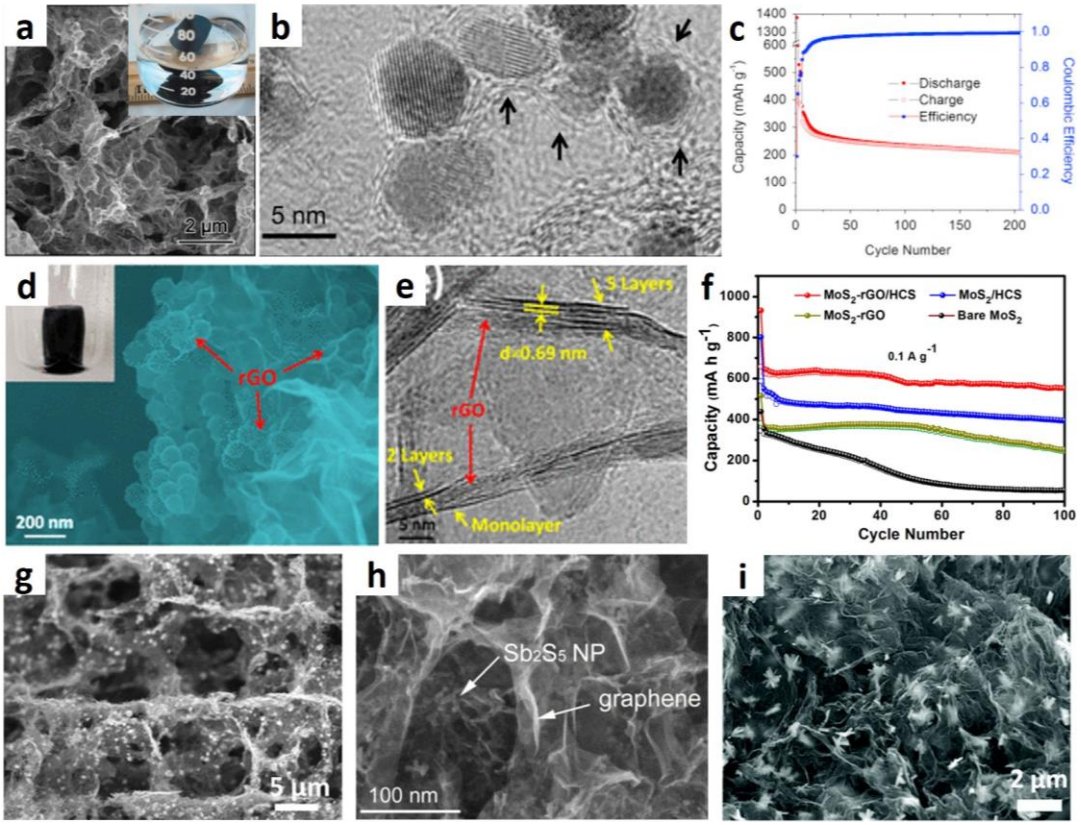

Figure 8. (a) SEM image with photograph (inset) and (b) TEM image of SnO_2-graphene dual aerogel, and (c) its cycling performance as anode for SIBs;[109] Reproduced with permission, Copyright 2015, Elsevier. (d) SEM image with photograph (inset) and (e) TEM image of graphene/MoS_2 aerogel, and (f) its cycling performance as anode for SIBs;[113] Reproduced with permission, Copyright 2018, American Chemical Society. (g) SEM image of graphene-WS_2 composite;[114] Reproduced with permission, Copyright 2016, John Wiley and Sons. (h) TEM image of 3D graphene-Sb_2S_5 aerogel;[111] Reproduced with permission, Copyright 2016, American Chemical Society. (i) SEM image of graphene-Bi_2S_3 aerogel.[115] Reproduced with permission, Copyright 2017, Royal Society of Chemistry.

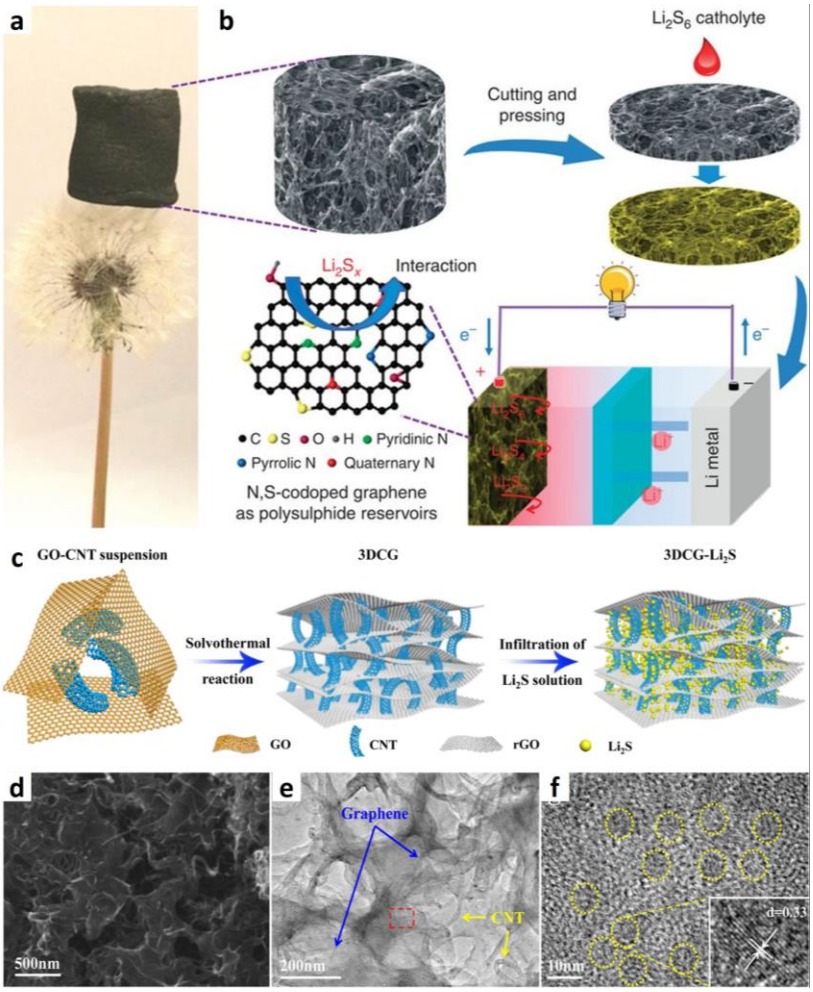

Figure 9. (a) Digital photograph of the doped graphene sponge; (b) Preparation of lithium polysulfide-graphene sponge composite cathode and its working principles.[123] Copyright 2015, Springer Nature. (c) Synthetic procedure for the 3D CNT/graphene-Li_2S composite, (d) SEM image of 3D CNT/graphene-Li_2S composite; (e) Low-magnification TEM image of 3D CNT/graphene-Li_2S, (f) TEM image of Li_2S nanoparticles on 3D CNT/graphene-S and high-resolution TEM image of Li_2S nanocrystals (inset).[131] Reproduced with permission, Copyright 2016, American Chemical Society.

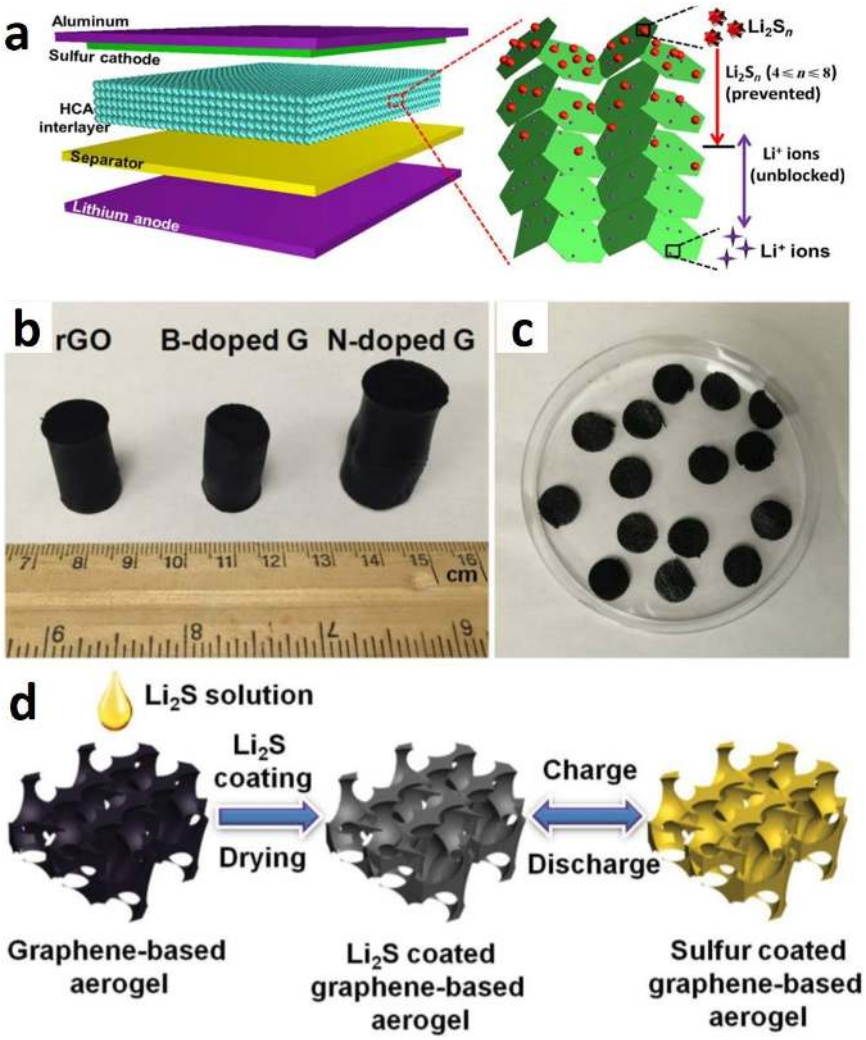

Figure 10. (a) Schematic illustration of the structure of a Li-S battery with an HCA interlayer and its inhibitory effect on the diffusion of polysulfides;[132] Reproduced with permission, Copyright 2016, Elsevier. (b) Photographs of the rGO, B-doped graphene, and N-doped graphene hydrogels after the hydrothermal reaction (the unit is centimeters for the upper scale); (c) Slices of the B-doped graphene hydrogel, (d) Schematic illustration of the Li_2S coating process and the in-situ charge/ discharge process of the graphene-based electrode.[144] Reproduced with permission, Copyright 2016, John Wiley and Sons.

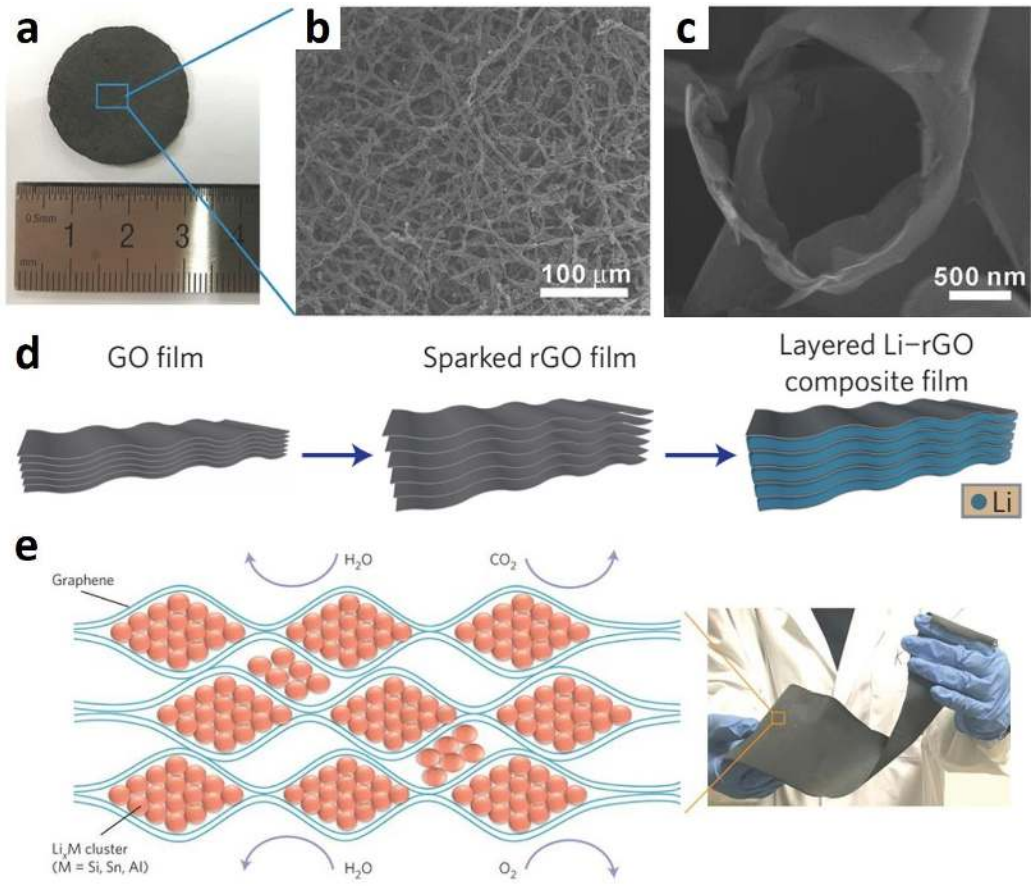

Figure 11. (a) Photograph of the 3DGA for lithium metal anode; (b) SEM image of the 3DGA; (c) SEM image showing the open end of a microtube.in 3DGA;[151] Reproduced with permission, Copyright 2017, John Wiley and Sons. (d) Schematic illustration of synthetic procedures, from a GO film (left) to a sparked rGO film (middle), to a layered Li-rGO composite film (right),[152] Reproduced with permission, Copyright 2016, Springer Nature. (e) Schematic illustration of the unique foil structure, comprising densely packed reactive Li_xSi nanoparticles encapsulated by large graphene sheets.[153] Reproduced with permission, Copyright 2017, Springer Nature.

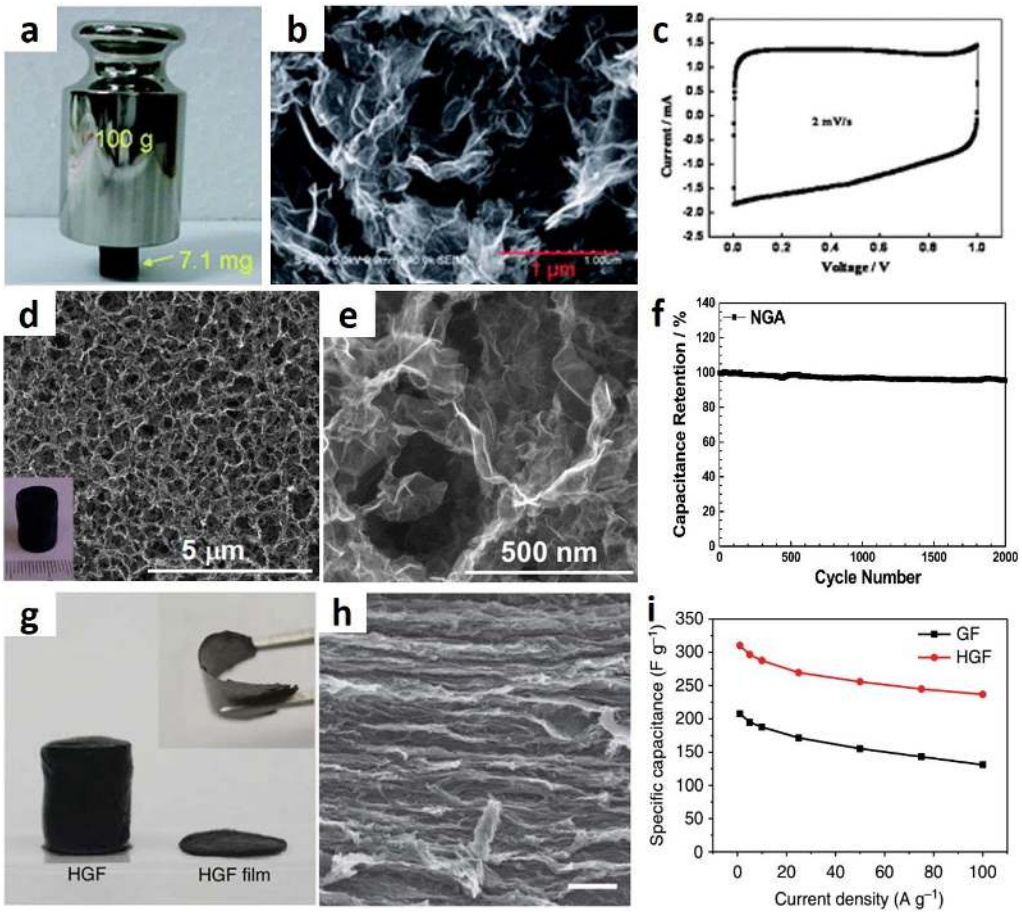

Figure 12. (a) Photograph and (b) SEM image of 3DGA for EDLCs, and (c) its CV curves;[9] Reproduced with permission, Copyright 2011, Royal Society of Chemistry. (d) Low magnification SEM image and photograph (inset), and (e) high-magnification SEM image of NGA; (f) Capacity retention of NGA electrode for EDLCs;[163] Reproduced with permission, Copyright 2015, American Chemical Society. (g) Photograph of HGF and pressed HGF film, (h) SEM image of pressed film, (i) Rate performance of HGF electrode.[164] Reproduced with permission, Copyright 2014, Springer Nature.

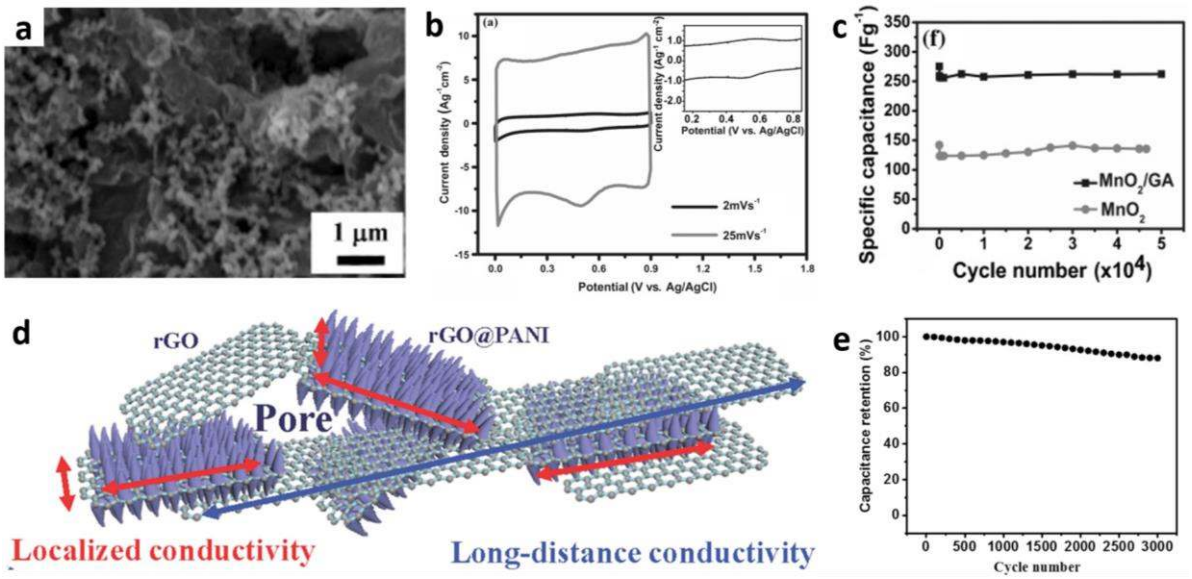

Figure 13. (a) SEM image of MnO_2/GA composite, (b) CV curves and enlarged CV curves (inset) of MnO_2/GA as electrode for supercapacitors, (c) Cycling performance of MnO_2/GA composite in comparison with MnO_2;[165] Reproduced with permission, Copyright 2013, John Wiley and Sons. (d) Schematic illustration of 3D graphene/PANI composite electrode, (e) Capacity retention of graphene/PANI electrode.[166] Reproduced with permission, Copyright 2018, Elsevier.

Table 1. Performance comparison of different 3DGAs and 3DGA-based composites for LIB/SIB applications.

Application	Materials	Current density (mA g^{-1})	Cycle number	Capacity	Voltage Range (V)	ICE (%)	Ref.
LIBs	3D graphene foam	2000	600	342 mAh g^{-1}	3-0.01	61.3	75
	SGFs	5000	500	404.5 mAh g^{-1}	3-0.01	48.5	78
	3DG@Fe_3O_2	200	130	1135 mAh g^{-1}	3-0.01	62.8	89
	MGAP	100	700	101.1 % retention	3-0.01	95.4	90
	V_2O_5@3DNG	100	100	235 mAh g^{-1}	4-2	~ 99	91
	Fe_3O_4@GS/GF	93	150	1059 mAh g^{-1}	3-0.01	~ 70	93
	Co_3O_4@NGN	1000	400	676 mAh g^{-1}	3-0.01	52.3	12
	C-MoS_2/N-G	200	500	900 mAh g^{-1}	3-0.01	70	98
SIBs	N-doped 3D rGO aerogel	100	200	287.9 mAh g^{-1}	3-0.01	~ 28	76
	HPGM	500	1600	~ 82 mAh cm^{-2}	4-1.5	N/A	77
	C@P/GA	2600	200	1096 mAh g^{-1}	2-0.01	70.5	103
	SnO_2-graphene dual aerogel	200	200	221 mAh g^{-1}	2.5-0.01	28.7	109
	Graphene/MoS_2 aerogel	100	100	1145 mAh g^{-1}	3-0.01	73	113
	Grapene-CNT-WS_2 aerogel	200	100	253 mAh g^{-1}	3-0.01	33.9	114
	Graphene-Sb_2S_5 aerogel	100	100	828 mAh g^{-1}	3-0.01	73.6	111
	Bi_2S_3-graphene aerogels	100	120	348 mAh g^{-1}	3-0.01	N/A	115

Table 2. Performance comparison of different 3DGAs and 3DGA-based composites for Li-S battery application.

Materials	Current density	Cycle number	Capacity	Voltage Range (V)	Cathode loading	Ref.
3D graphene sponge	0.5 C	200	670 mAh g^{-1}	2.8-1.5	4.6 mg cm^{-2}	123
S-r-GO	0.1 C	75	3 mAh cm^{-2}	2.8-1.7	67 wt%	124
3DCG-Li_2S	0.2 C	300	958.3 mAh g^{-1}	3-1.5	81.4 wt%	131
HCA-S	4 C	600	78% capacity retention	3-1.7	N/A	132
Py-GF@S	0.5 C	100	798 mAh g^{-1}	3-1.5	6.2 mg cm^{-2}	137
GA/TiO_2/S	1 C	250	512 mAh g^{-1}	2.8-1.7	1.1-1.3 mg cm^{-2}	138
ZnO/G-S	0.2 C	100	752 mAh g^{-1}	2.8-1.5	1-1.2 mg cm^{-2}	139
MgO/G-S	0.2 C	100	767 mAh g^{-1}	2.8-1.5	1-1.2 mg cm^{-2}	139
Li_2S@Li_3PS_4/GA	0.1 C	100	485.5 mAh g^{-1}	2.8-1.5	1.2 mg cm^{-2}	140
Li_2S/B-doped graphene	0.5 C	300	403 mAh g^{-1}	2.8-1.7	1.8-2.3 mg cm^{-2}	144
Li_2S/N-doped graphene	0..5 C	300	357 mAh g^{-1}	2.8-17	1.8-2.3 mg cm^{-2}	144

Table 3. Performance comparison of different 3DGAs and 3DGA-based composites for supercapacitor application.

Materials	Current density	Capacitance	Cycle number	Retention	Voltage Range (V)	Electrolyte	Ref.
Supercritical CO_2 dried GA	50 mA g^{-1}	128 F g^{-1}	N/A	N/A	1-0	6M potassium hydroxide (KOH)	9
NGA	0.2 A g^{-1}	223 F g^{-1}	2000	92 % (1 A g^{-1})	1-0	1M H_2SO_4	163
HGF	1 A g^{-1}	298 F g^{-1} 212 F cm^{-3}	10000	91 % (20 A g^{-1})	3.5-0	$EMIMBF_4$/AN	164
MnO_2/GA	1 V s^{-1}	264 F g^{-1}	50000	84 % (1 V s^{-1})	0.9-0	0.5 M Na_2SO_4	165
HGC-PANI	5 mV s^{-1}	453 mF cm^{-2}	3000	90 % (0.1 V s^{-1})	1-0	PVA-H_2SO_4 (solid state)	166
3D-GCA	0.4 A g^{-1}	4.76 F g^{-1}	10000	95.5 % (200 mV s^{-1})	0.8-0	3M KOH	65
V_3S_4/3DGH	10 mV s-1	225 F g^{-1}	5000	98.3 (100 mV s^{-1})	0.8-0	5 M LiCl	51

In this paper, we review recent advances in synthesizing 3D graphene architectures and their composites, as well as their application in different energy storage devices, including various battery systems and supercapacitors. In addition, their challenges for application at the current stage are discussed, and future development prospects are indicated.

Keywords: 3D graphene architectures, hybrid structures, electrodes, energy storage

Authors: Zhijie Wang, Hong Gao, Qing Zhang, Yuqing Liu, Jun Chen* and Zaiping Guo*